DOT1L regulates chromatin reorganization and gene expression during sperm differentiation

Mélina Blanco[1], Laila El Khattabi[1,2*], Clara Gobé[1*], Marion Crespo[3,4], Manon Coulée[1], Alberto de la Iglesia[1,5], Côme Ialy-Radio[1], Clementine Lapoujade[6], Maëlle Givelet[6], Marion Delessard[1], Ivan Seller-Corona[1] , Kosuke Yamaguchi[7], Nadège Vernet[8], Fred Van Leeuwen[9], Alban Lermine[10], Yuki Okada[7], Romain Daveau[10], Rafael Oliva[5,11], Pierre Fouchet[6], Ahmed Ziyyat[1,12], Delphine Pflieger[3], and Julie Cocquet[1,13]

1 Université Paris Cité, INSERM, CNRS, Institut Cochin, F-75014 Paris, France.

2 Sorbonne Université and APHP, Hôpital Armand Trousseau, Chromosomal genomics unit, Medical genetics department, F-75012 Paris, France.

3 University Grenoble Alpes, CEA, INSERM, UA13 BGE, CNRS, CEA, FR2048, Grenoble, France

4 ADLIN Science, Pépinière « Genopole Entreprises », Evry, France.

5 Molecular Biology of Reproduction and Development Research Group, Department of Biomedical Sciences, Faculty of Medicine and Health Sciences, Institut d'Investigacions Biomèdiques August Pi I Sunyer (IDIBAPS), Fundació Clínic per a la Recerca Biomèdica, Universitat de Barcelona (UB), Barcelona, Spain.

6 Université de Paris and Université Paris-Saclay, iRCM/IBFJ CEA, UMR Stabilité Génétique Cellules Souches et Radiations, Laboratoire des Cellules Souches Germinales, F-92265, Fontenay-aux-Roses, France.

7 Institute for Quantitative Biosciences, The University of Tokyo, Tokyo 113-0032, Japan.

8 Institut de Génétique et de Biologie Moléculaire et Cellulaire (IGBMC), Département de Génétique Fonctionnelle et Cancer, CNRS, INSERM, Université de Strasbourg, 1 rue Laurent Fries, F-67404 Illkirch, France.

9 Division of Gene Regulation, Netherlands Cancer Institute, 1066CX, Amsterdam, The Netherlands.

10 MOABI-APHP Bioinformatics Platform-I&D-DSI, Assistance Publique-Hôpitaux de Paris, Paris, France.

11 Biochemistry and Molecular Genetics Service, Clinic Barcelona, Spain.

12 Service d'Histologie, d'Embryologie, Biologie de la Reproduction, AP-HP, Hôpital Cochin, F-75014 Paris, France.

13 Lead contact. Correspondence: julie.cocquet@inserm.fr

*equal contribution

Abstract

Spermatozoa have a unique genome organization: their chromatin is almost completely devoid of histones and is formed instead of protamines which confer a high level of compaction and preserve paternal genome integrity until fertilization. Histone-to-protamine transition takes place in spermatids and is indispensable for the production of functional sperm. Here we show that the H3K79-methyltransferase DOT1L controls spermatid chromatin remodelling and subsequent reorganization and compaction of spermatozoon genome. Using a mouse model in which *Dot1l* is knocked-out (KO) in postnatal male germ cells, we found that *Dot1l*-KO sperm chromatin is less compact and has an abnormal content, characterized by the presence of transition proteins, immature protamine 2 forms and a higher level of histones. Proteomics and transcriptomics analyses performed on spermatids reveal that *Dot1l*-KO modifies the chromatin prior to histone removal, and leads to the deregulation of genes involved in flagellum formation and apoptosis during spermatid differentiation. As a consequence of these chromatin and gene expression defects, *Dot1l*-KO spermatozoa have less compact heads and are less motile which results in impaired fertility.

Keywords

DOT1L, H3K79 methylation, spermatogenesis, gene regulation, histone-to-protamine transition, chromatin compaction, flagellum development

58 ## Introduction

59 During the postmeiotic phase of spermatogenesis, male germ cells known as spermatids
60 undergo profound morphological and functional changes to differentiate in spermatozoa. This process
61 is driven by a rich genetic program characterized by the expression of thousands of genes in round
62 spermatids (Chen *et al*, 2018; da Cruz *et al*, 2016; Ernst *et al*, 2019; Green *et al*, 2018; Soumillon *et al*,
63 2013). Then, when spermatids elongate, their chromatin is extensively remodeled which ultimately
64 results in the eviction of ~85-99 % of nuclear histones and their replacement by more basic, smaller
65 proteins, called protamines [for reviews, see (Bao & Bedford, 2016; Rathke *et al*, 2014)]. This unique
66 chromatin reorganization induces a 6-10 times higher level of compaction of the spermatozoon
67 chromatin compared to the canonical nucleosome-based chromatin (Ward & Coffey, 1991). Non-
68 histone packaging of male germ cell genome is conserved throughout evolution and expected to be
69 important to protect paternal DNA from damages and prepare its reprograming in the zygote, if
70 fertilization occurs (Rathke *et al.*, 2014). A compact genome is also an advantage for the motile
71 spermatozoa as it is compatible with a smaller and more hydrodynamic head (Braun, 2001).

72 In the past decades, the molecular mechanisms driving histone eviction and subsequent
73 compaction of the sperm genome have been the focus of several studies which have demonstrated
74 the essential role of transition proteins (Zhao *et al*, 2004a; Zhao *et al*, 2004b), of histone variants (Barral
75 *et al*, 2017; Montellier *et al*, 2013), of histone post-translational modifications (PTMs), in particular
76 hyperacetylation (Goudarzi *et al*, 2016; Oliva *et al*, 1987), and of writers and readers of histone
77 acetylation (Dong *et al*, 2017; Gaucher *et al*, 2012; Luense *et al*, 2019; Shang *et al*, 2007; Shiota *et al*,
78 2018). Interestingly, high levels of histone H3 Lysine 79 di- and tri-methylation (H3K79me2 and me3)
79 have been observed at the same time as histone hyperacetylation, just prior to histone removal
80 (Dottermusch-Heidel *et al*, 2014a; Dottermusch-Heidel *et al*, 2014b; Moretti *et al*, 2017) (Fig 1A), but
81 their biological significance remains to date unknown. H3K79 methylation is mediated by one enzyme,
82 encoded by the gene *Dot1l*, of which pattern of expression and sequence are conserved from
83 Drosophila to mammals. *Dot1l* has been implicated in development, cell reprogramming,
84 differentiation and proliferation [for review, see (Kim *et al*, 2014; Vlaming & van Leeuwen, 2016)]. It
85 has recently been found to be essential for spermatogonial stem cell self-renewal (Lin *et al*, 2022) but
86 its role in postmeiotic male germ cells, where it is the most highly expressed (Dottermusch-Heidel *et*
87 *al.*, 2014a; Dottermusch-Heidel *et al.*, 2014b; Moretti *et al.*, 2017), has not been addressed.

88 In the present paper, we investigated *Dot1l* role in postmeiotic cells by a comprehensive
89 analysis of the phenotypic and molecular consequences of its knockout in mouse male germ cells. We
90 found that *Dot1l* is required for gene regulation and chromatin reorganization in spermatids and that
91 its knockout leads to the production of abnormally shaped nonfunctional spermatozoa with a deficient
92 chromatin and nucleus compaction.

93 # Results

94

95 ***Dot1l* is essential for spermatogenesis and male fertility**

96 In both mouse and human, *Dot1l/DOT1L* gene is highly expressed in the testis (Appendix FigS1A). More
97 precisely, it is expressed in all testicular cells with a strong expression at postnatal stage in meiotic cells
98 (spermatocytes) and postmeiotic cells (spermatids) (Appendix FigS1A-C) (Dottermusch-Heidel *et al.*,
99 2014a; Dottermusch-Heidel *et al.*, 2014b; Green *et al.*, 2018; Moretti *et al.*, 2017). To investigate the
100 role of *Dot1l* in male germ cells, we generated a conditional knockout using *Stra8-Cre r*ecombinase
101 (Sadate-Ngatchou *et al*, 2008) and a mouse transgenic line in which *Dot1l* exon 2 is flanked by LoxP
102 sites (Jo *et al*, 2011) (Appendix FigS1D). Previous studies have reported that *Stra8-Cre* is specifically
103 expressed in the male germline where it is expressed from postnatal day 3 and CRE recombinase
104 reaches maximum efficiency in pachytene spermatocytes (Bao *et al*, 2013; Sadate-Ngatchou *et al.*,
105 2008). Bao *et al.* have also observed that *Stra8-Cre* is more efficient at cutting one allele rather than
106 two (Bao *et al.*, 2013). We therefore generated mice in which one allele of *Dot1l* is floxed and one allele
107 is already deleted (Δ) to increase efficiency of floxed exon excision upon *Cre* recombinase expression
108 (*Dot1l*$^{Fl/\Delta}$*; Stra8-Cre* mice, hereafter called *Dot1l*-KO or KO). First, to estimate the efficiency of *Dot1l*
109 knockout, we detected DOTL1 protein by western blot and immunochemistry on adult testes from
110 *Dot1l*-KO (*Dot1l*$^{Fl/\Delta}$*; Stra8-Cre*) and controls (*Dot1l*$^{Fl/Fl}$) (Figs 1B-C and Appendix FigS1E-G). We found a
111 reduction of >85 % of DOT1L signal but not complete abolishment/knockout of DOT1L level, despite
112 strong activity of *Stra8-Cre* in most adult germ cells (Appendix FigS1H). Analyses of purified germ cell
113 fractions confirmed reduced level but not complete absence of DOTL1 protein, along with a reduction
114 of H3K79me2 level (Figs 1D, EV1 and Appendix FigS1I). Multiple protein isoforms of DOT1L have been
115 described in the literature and several of them were observed in our western blots, including the
116 canonical (~165 kDa) and testis-specific (~185 kDa) isoforms (Dottermusch-Heidel *et al.*, 2014b; Zhang
117 *et al*, 2004), as well as less studied isoforms such as Q679P5 (~122KDa) or Q6XZL7 (~68KDa)
118 (https://www.uniprot.org). All of them were markedly reduced in *Dot1l*-KO testicular extracts
119 (Appendix FigS1E and I).

120 To investigate the impact of *Dot1l* knockout on spermatogenesis and male fertility, the reproductive
121 parameters of adult *Dot1l*-KO males were investigated: significant decreases in testis weight and sperm
122 count were observed (independently of body weight, Fig 2A and Appendix FigS2A-B). Histological
123 analyses revealed the presence of "empty" tubules without germ cells or missing germ cell layers (Fig
124 2B and Appendix FigS2C) highlighting a spermatogonial defect as described by Lin et al (Lin *et al.*, 2022).
125 However, there was no homogenous blockage/arrest at a specific stage of *Dot1l*-KO spermatogenesis.

126 These observations were confirmed by cytometry analyses in which the number of all germ cell
127 populations (i.e. spermatogonia with Side Population phenotype, spermatocytes and spermatids) was
128 found decreased in *Dot1l*-KO testes (Fig 2C), but their frequency was not altered (Appendix FigS2F).
129 Collectively, these data show that the *Dot1l*-KO we produced does not lead to a spermatogenesis
130 arrest. When mated to WT females, *Dot1l*-KO males were found to be hypofertile with significant
131 reductions in the number of litters and in litter size compared to that of control (CTL) males (Fig 2D
132 and Appendix FigS2D-E). We genotyped the few pups obtained and observed that the floxed allele was
133 transmitted to 35% of babies (12 out of 34) and the deleted allele to 65% of them. This indicates that
134 the deleted allele can be transmitted but less efficiently than what was expected based on our
135 quantification of *Dot1l*-KO spermatids by immunofluorescence (i.e. only 65% of transmission of the
136 deleted allele although >85% of spermatids were devoid of DOT1L protein).

137 The reduction in litter number and size could result from impaired fertilizing ability of *Dot1l*-KO sperm
138 or from a developmental defect. To address this question, we measured the fertilization rate 24h after
139 WT females were mated with *Dot1l*-KO or CTL males. The numbers of fertilized and non-fertilized
140 oocytes collected in the oviduct ampulla were counted in both groups (a total of 113 oocytes were
141 analyzed from 9 WT females mated with 4 CTL, and 73 oocytes from 6 WT females mated with 3 KO).
142 A significant reduction in the fertilization rate was observed for *Dot1l*-KO indicating that *Dot1l*-KO
143 sperm are less functional than CTL sperm (Fig 2E). In addition to *in vivo* fertility monitoring, we
144 performed *in vitro* fertilization (IVF) assays using the same number of spermatozoa per experiment.
145 Using spermatozoa from *Dot1l*-KO males, no oocyte was fertilized *in vitro*, while spermatozoa from
146 control males (including WT, CTL and HET males) led to the fertilization of ~37% of oocytes (Fig 2E, and
147 see Appendix FigS2G for individual values). When using oocytes devoid of zona pellucida, in order to
148 bypass the zona pellucida crossing step, spermatozoa from *Dot1l*-KO males still performed very poorly
149 compared to that of CTL males (~3 % of fertilized oocytes using *Dot1l*-KO sperm compared to ~88 %
150 for CTL, Fig 2E), confirming that *Dot1l*-KO dramatically reduces sperm fertilizing ability. IVF is known to
151 be less efficient and to lead to lower fertilization rates than in vivo. It is therefore more sensitive to
152 sperm defects, as observed in other studies (Barraud-Lange *et al*, 2020; Gadadhar *et al*, 2021;Fujihara
153 *et al*, 2010; Kawano *et al*, 2010).

154

155 ***Dot1l*-KO disrupts spermiogenesis and leads to the production of malformed nonfunctional**
156 **spermatozoa**

157 To determine the reason why *Dot1l*-KO spermatozoa are less functional than CTL ones, we investigated
158 their morphology and motility. Spermatozoa are highly specialized cells characterized by a small head

159 which encompasses their very compact nucleus, a long flagellum that confers motility and almost no
160 cytoplasm. First, we observed that *Dot1l*-KO epididymal spermatozoa displayed malformed heads and
161 abnormal flagella (characterized by thinning of some sections in their midpiece) (Figs 3A and EV2A).
162 Inside the flagellum, the axoneme normally contains a ring of nine outer microtubule doublets and two
163 central microtubules (9+2 axoneme). In *Dot1l*-KO sperm, ultrastructure analyses revealed abnormal
164 axonemes, characterized by disorganized microtubules (<9+2 microtubules) (Fig 3B). Nuclear
165 compaction was also found impaired, observed as less contrasted nuclei in KO in comparison with CTL
166 sperm. *Dot1l*-KO sperm also showed an increased cytoplasmic retention (Figs 3B and EV2A). Using
167 CASA (computer-assisted sperm analyses), we observed that *Dot1l*-KO sperm motility was impaired,
168 with a reduced proportion of motile and progressively motile (i.e. swimming in an overall straight line
169 or in very large circles) spermatozoa (Figs 3C and EV2B). This was not due to cell death as sperm vitality
170 was comparable between CTL and *Dot1l*-KO mice (Appendix FigS3A). Axoneme/flagellum organization,
171 nucleus compaction and cytoplasm elimination occur during the differentiation of spermatids in
172 spermatozoa (i.e. spermiogenesis). We measured apoptosis during this transition by TUNEL assay on
173 testicular sections, and found a higher incidence of apoptotic elongating/condensing spermatids in
174 *Dot1l*-KO than in CTL, another indication of a defective spermiogenesis (i.e. 6% of tubules containing
175 apoptotic elongating/condensing spermatids in CTL vs 40% of tubules in DOT1L-KO, p =0.0007, Fig 3D).
176 Collectively, our data indicate that *Dot1l*-KO spermiogenesis is impaired at multiple levels and
177 produces less functional spermatozoa.

178

179 **_Dot1l_-KO modifies the chromatin of postmeiotic male germ cells, which results in abnormal**
180 **chromatin reorganization and compaction in spermatozoa**
181

182 During spermiogenesis, spermatid chromatin undergoes specific reorganization and compaction as
183 most histones are removed and replaced with protamines (Bao & Bedford, 2016; Rathke *et al.*, 2014).
184 Histone variants (such as TH2B or H2AL2) and transition proteins (TNP) are highly expressed in
185 spermatids during histone-to-protamine transition and are essential for the correct reorganization and
186 compaction of the sperm genome with protamines (Barral *et al.*, 2017; Montellier *et al*, 2011). In
187 addition to the nuclear compaction defects observed by electron microscopy (Fig 3B), we noticed that
188 *Dot1l*-KO sperm chromatin is more sensitive to nucleoplasmin-induced decompaction than CTL sperm
189 chromatin. Nucleoplasmin, or NPM, is a histone chaperone known to facilitate paternal chromatin
190 decompaction and reorganization after fertilization owing to its ability to bind histones and sperm
191 nuclear basic proteins (Frehlick *et al*, 2007). Following NPM treatment, a higher proportion of soluble
192 histones was found in *Dot1l*-KO compared to CTL sperm (Appendix FigS3B) in agreement with a

193 chromatin compaction defect. We next quantified TH2B and H3 histones in epididymal spermatozoa
194 by western blot and, despite inter individual variability, we found significantly more residual histones
195 in *Dot1l*-KO than in CTL sperm chromatin (Figs 3E, 3H and Appendix FigS3C-D). We also quantified
196 transition protein 2 (TNP2) and found a clear retention of this protein in *Dot1l*-KO spermatozoa while
197 nothing could be detected in CTL sperm (Figs 3F, 3H and Appendix FigS3E). Finally, we quantified
198 protamines on acid-urea gels and observed an accumulation of immature (non-cleaved) forms of
199 Protamine 2 in *Dot1l*-KO spermatozoa vs. CTL (Fig 3G). A slight but significant distorted
200 Protamine1/Protamine2 (PRM1/PRM2) ratio was also observed in *Dot1l*-KO spermatozoa (Figs 3G-3H
201 and Appendix FigS3F).

202 The transition from nucleosomes to protamine-based chromatin starts in elongating spermatids with
203 the incorporation of histone post-translational modifications (PTMs) and histone variants [for reviews
204 see (Bao & Bedford, 2016; Oliva, 2006; Rathke *et al.*, 2014)]. To better understand how DOT1L impacts
205 on chromatin organization prior to histone removal, we quantified histone PTMs and variants by liquid
206 chromatography-tandem mass spectrometry (LC-MS/MS) in whole testes and in
207 elongating/condensing spermatids. In whole testis histone extracts we observed, as expected, a clear
208 decrease of H3K79 mono- and di-methylation in *Dot1l*-KO samples compared to CTL (Appendix FigS4A).
209 The tri-methylation of H3K79 was not detectable with this analysis, possibly due to its small
210 stoichiometry. No other significant differences in histone H3 PTMs were detected between *Dot1l*-KO
211 and CTL whole testicular histone extracts. However, a significant decrease in histone H4 hyper-
212 acetylated form (i.e. H4K5ac,K8ac,K12ac,K16ac) was observed (Appendix FigS4A). In
213 elongating/condensing spermatids (ES), the stage during which chromatin is extensively remodelled, a
214 significant decrease in H3K79 mono- and di-methylation levels was also observed (Fig 4A). Here also,
215 H3K79 tri-methylation was not detectable. Several other quantitative changes in histone PTMs were
216 observed such as modest increases in H3K23ac, H2AR88me1 and TH2BK35ac but also a dramatic
217 decrease of H4K20 or R23 mono-, di- and tri-methylated forms (Fig 4 and Appendix FigS4B).
218 Quantification of histone variants showed significant changes in H1 variants and in canonical H2A
219 (Appendix FigS4C). The most remarkable change was, as in whole testes, a severe decrease in H4
220 acetylation in *Dot1l*-KO elongating/condensing spermatids, in particular of hyper-acetylated forms
221 such as H4K5ac,K12ac,K16ac, H4K8ac,K12ac,K16ac and H4K5ac,K8ac,K12ac,K16ac (Fig 4B). In
222 elongating spermatids, histone H4 hyper-acetylation is an essential step of histone-to-protamine
223 transition, as it facilitates chromatin loosening and nucleosome disassembly prior to histone removal
224 [for review see (Oliva, 2006)]. By western blot and immmunofluorescence, we also observed a
225 decrease in H4 acetylation in *Dot1l*-KO elongating/condensing spermatids compared to CTL using anti-
226 H4K16ac or anti-poly H4ac antibody (Fig EV3 and Appendix FigS4D).

227 We next quantified histone PTMs and variants at an earlier stage of spermiogenesis, in round
228 spermatids (RS), and did not see any decrease in H4 acetylation or H4K20 methylation in KO vs. CTL RS
229 (Fig EV4) in contrast with what was observed in ES (Fig 4). Apart from the expected decrease in H3K79
230 methylation, the only quantitative changes that were detected in RS were increases in H3K18
231 crotonylation (H3K18cr), in H4K8cr,K12ac,K16ac and in H1 variants (Fig EV4 and Appendix FigS4C,E). In
232 spermatozoa, some H3K79 methylation has been detected on persistent histones (Luense *et al*, 2016;
233 Moretti *et al.*, 2017) and a significant decrease in H3K79me1 and H3K79me2 levels was visible in *Dot1l*-
234 KO spermatozoa using LC-MS/MS. Apart from a modest increase in H3K18ac, no other changes were
235 detected at this stage (Appendix FigS4F).

236 All these observations indicate that *Dot1l* KO has a profound impact on postmeiotic chromatin in ES at
237 the time of its reorganization, which disrupts histone-to-protamine transition and leads to a higher
238 proportion of retained histones, transition proteins and unprocessed protamine 2 in spermatozoa.

239

240 **DOT1L regulates the expression of genes involved in essential processes of spermatid differentiation**

241 In order to gain insight into the gene expression changes associated with *Dot1l* deficiency in male germ
242 cells, we performed RNA-Seq analyses on purified germ cells from 3 different spermatogenic stages,
243 each in 5 replicates: primary spermatocytes (SC), secondary spermatocytes (SCII) and round
244 spermatids (RS) (Fig 5A). We did not include elongating/condensing spermatids in this analysis because
245 their transcriptome is very similar to that of round spermatids, and, at this stage, transcription
246 progressively shuts down as a consequence of histone-to-protamine transition and genome
247 compaction. RNA-Seq differential analyses showed hundreds of significantly deregulated genes in
248 *Dot1l*-KO vs CTL samples (DEseq2, with a Fold change > 1.5 and FDR < 0.05). In parallel, we performed
249 a less stringent analysis (DEseq2, with a Fold change > 1.5 and $p < 0.05$, then *a posteriori* validation of
250 FDR) and found between ~600 and 1000 deregulated genes at each stage (Fig 5B and Appendix FigS5A).
251 With both analyses, the number of deregulated genes increased with progression of male germ cell
252 differentiation and was therefore highest in RS (Fig 5B and Appendix FigS5A), and approximately half
253 of deregulated genes were found in common in at least 2 stages (Appendix FigS5A). In the three cell
254 types, more genes were found upregulated than downregulated in KO samples (Fig 5B) in agreement
255 with results obtained recently in *Dot1l*-KO somatic cells (Aslam *et al*, 2021; Cattaneo *et al*, 2022). To
256 link gene deregulation in *Dot1l*-KO mice with DOT1L methyltransferase activity, we compared
257 deregulated genes with the genomic location of H3K79me2 that we obtained by ChIP-seq in RS.
258 H3K79me2 is the best characterized H3K79 methylation mark and is known to mark the body of
259 transcriptionally active genes. H3K79me1 and me3 have similar trends, though broader for the former,

260 and more restricted for the latter (Vlaming & van Leeuwen, 2016). Here, in wild type RS, H3K79me2
261 was found enriched at the body (with the strongest signal found near the Transcriptional Start Site) of
262 genes which were downregulated in the KO but not those found upregulated (Fig 5C and Appendix
263 FigS5B). Observation of ChIP peaks confirmed the presence of H3K79me2 mark at down but not
264 upregulated genes (Fig 5D).

265 We next investigated deregulated pathways using GSEA (Gene Set Enrichment Analysis), a threshold-
266 free method which considers all genes based on their differential expression rank, and found a
267 downregulation of biological pathways related to apoptosis, transcription/RNA regulation,
268 chromatin/chromosome organization and mitochondria activity in *Dot1l*-KO vs. CTL round spermatids
269 (Fig 5E). Prior to spermiogenesis, pathways related to cilium or flagellum motor activity were found
270 downregulated in *Dot1l*-KO primary spermatocytes while, in *Dot1l*-KO secondary spermatocytes,
271 pathways related to chromatin/chromosome organization were the most significantly deregulated (Fig
272 5E). When looking at gene ontology for "cellular components", pathways related to ribosomal
273 structure or to mitochondrial proteins were found deregulated in RS (Fig EV5). Strikingly, several *Slc*
274 genes were found deregulated in *Dot1l*-KO RS (Appendix FigS5C). *Slc* genes encode solute carriers, and
275 several of them have been implicated in sperm motility *via* their effects on flagellum differentiation
276 and/or sperm energy production (Kuang *et al*, 2021; Maruyama *et al*, 2016; Toure, 2019).

277 In agreement with the downregulation of pathways related to apoptosis, *Bcl6*, *Jak3* and *Tsc22d3* which
278 encode proteins with anti-apoptotic effects (Aguilar *et al*, 2014; Kurosu *et al*, 2003; Thomis *et al*, 1997)
279 were found significantly downregulated in RS. *Blc6* codes for a transcription repressor (Chang *et al*,
280 1996) and appears to be a direct target of DOT1L since it is downregulated upon *Dot1l* loss, and
281 enriched in H3K79me2 in wild-type RS (Fig 5E). Interestingly, an unsupervised search for DNA motifs
282 identified BCL6/BCL6B DNA binding site as the most significantly enriched motif in the promoter of
283 upregulated genes (15 upregulated genes, Appendix FigS5D). This finding is in agreement with a model
284 in which downregulated genes are direct H3K79me2/DOT1L targets while upregulated genes are
285 indirect targets.

286

287 # Discussion
288

289 In the present study, using a conditional knockout mouse model, we demonstrate that the H3K79
290 methyltransferase DOT1L is essential for gene regulation and chromatin remodelling during spermatid
291 differentiation.

292 DOT1L is highly conserved among eukaryotes. In mammalian it has been extensively studied and found
293 to be involved in many different biological processes such as mixed lineage leukaemia (Nguyen *et al*,
294 2011; Okada *et al*, 2005), cell cycle (Kim *et al.*, 2014), development (Jones *et al*, 2008), reprogramming
295 (Onder *et al*, 2012), DNA damage repair (Lin *et al*, 2009; Zhu *et al*, 2018) or transcription activation
296 (Steger *et al*, 2008; Wang *et al*, 2008). In the male germline, DOT1L is highly expressed at the RNA and
297 protein levels, in particular in postmeiotic cells (Dottermusch-Heidel *et al.*, 2014a; Dottermusch-Heidel
298 *et al.*, 2014b; Moretti *et al.*, 2017). Before meiosis, DOTL1 has been found to be required for the self-
299 renewal of adult stem cells. Indeed, with a *Dot1l* KO induced by a Cre recombinase expressed earlier
300 than the one used in the present study, Lin et al. observed a progressive (age-dependent) loss of all
301 male germ cell types, ultimately resulting in a Sertoli cell only syndrome (i.e. absence of germ cells)
302 (Lin *et al.*, 2022). In the *Dot1l*-KO males we characterized here, we also found empty tubules as well as
303 a decrease of all germ cell types, but milder, which enabled us to address the role of DOT1L in adult
304 postmeiotic germ cells (i.e. spermatids). Strikingly, we found that *Dot1l*-KO spermatozoa present
305 multiple anomalies such as thinner and distorted flagella, cytoplasmic retention and impaired nuclear
306 compaction. As a result, KO spermatozoa are less motile and their fertilizing ability is compromised.
307 These defects are associated with the deregulation of hundreds of genes in *Dot1l*-KO meiotic and
308 postmeiotic germ cells. Previous studies have shown that spermatid differentiation is associated with
309 the specific expression (or highly enriched expression) of thousands of genes, and that this genetic
310 program starts as early as in primary spermatocytes (Chen *et al.*, 2018; da Cruz *et al.*, 2016; Ernst *et*
311 *al.*, 2019; Green *et al.*, 2018; Soumillon *et al.*, 2013). Here, our analyses indicate that pathways related
312 to "cilium/flagellum assembly or motility" are deregulated from the spermatocyte stage, and those
313 related to "nucleosome assembly, chromatin remodelling" are deregulated in secondary
314 spermatocytes and round spermatids. A significant proportion of *Dot1l*-KO spermatids undergo
315 apoptosis and this was also visible by RNA-Seq with the deregulation of "apoptosis" related pathways
316 in RS, including the downregulation of genes with anti-apoptotic effects such as *Bcl6* or *Jak3* (Kurosu
317 *et al.*, 2003; Thomis *et al.*, 1997). Interestingly, several potential BCL6 target genes were identified
318 among the genes which are upregulated in *Dot1l*-KO spermatids. Like other upregulated genes, most
319 of them are devoid of H3K79me2 in wild type spermatids and may not be directly regulated by DOT1L.
320 In contrast, *Bcl6* and many other downregulated genes in *Dot1l*-KO spermatids are marked by

321 H3K79me2 in wild-type cells and are likely directly regulated by DOT1L. Our findings are in agreement
322 with recent studies in which *Dot1l* knockout was investigated in B cells, T cells or cardiomyocytes. Each
323 time, H3K79me2 was found to be enriched at the body of downregulated genes but not of upregulated
324 genes (Aslam *et al.*, 2021; Cattaneo *et al.*, 2022; Kwesi-Maliepaard *et al*, 2020).

325 Strikingly, many genes encoding members of the solute carrier family were deregulated in *Dot1l*-KO
326 male germ cells. Several members of this family such as *Slc22a14* and *Slc26a8* have previously been
327 implicated in sperm motility *via* their effects on flagellar differentiation and/or sperm energy
328 production (Kuang *et al.*, 2021; Maruyama *et al.*, 2016; Toure, 2019); the deregulation of *Slc* genes
329 with similar function could therefore contribute to the sperm flagellar and motility defects of *Dot1l*-
330 KO males. Overall, these data indicate that *Dot1l*-KO-induced gene deregulation is responsible for the
331 multiple defects of postmeiotic male germ cell differentiation.

332 In addition to being involved in the regulation of spermatid gene expression, we show that DOT1L is
333 essential for spermatid chromatin remodelling and subsequent reorganization and compaction of
334 spermatozoon genome. Indeed, the chromatin of *Dot1l*-KO spermatozoa is less compact, and
335 characterized by a higher level of retained histones, of transition protein 2 and of immature forms of
336 protamine 2, as well as altered protamine 1/2 ratio. Several other studies have observed similar
337 anomalies in particular retained histones and immature forms of protamine 2, as a result of
338 incomplete histone-to-protamine transition, such as *Tnp1*-KO (*transition protein 1*) (Yu *et al*, 2000),
339 *H2al2*-KO (*H2A histone family member L2A*) (Barral *et al.*, 2017), deletion of the mouse Y chromosome
340 long arm (Yamauchi *et al*, 2010), or *Kat2a* –KO (a.k.a. *Gcn5)* which encodes the lysine acetyltransferase
341 2A (Luense *et al.*, 2019). Similarly, a recent study has shown that aberrant pre-PRM2 cleavage leads to
342 altered levels of histone variants and transition proteins in sperm (Arevalo *et al*, 2022). In all those
343 mouse models as well as in the *Dot1l*-KO presented here, abnormal sperm chromatin content is
344 associated with fertility problems. This is also the case in humans, since impaired protamine 1/2 ratio
345 and accumulation of pre-PRM2 are associated with male infertility (de Mateo *et al*, 2009; Torregrosa
346 *et al*, 2006).

347 In elongating spermatids, histones – in particular histone H4 – are hyper-acetylated prior to their
348 replacement. This phenomenon is a prerequisite for histone-to-protamine transition as it creates a
349 permissive state for histone removal [for reviews see (Bao & Bedford, 2016; Oliva, 2006; Rathke *et al.*,
350 2014)]. H3K79me2/3 levels peak at the time of H4 hyperacetylation (Dottermusch-Heidel *et al.*, 2014a;
351 Dottermusch-Heidel *et al.*, 2014b; Moretti *et al.*, 2017) and we show here that both H3K79 methylation
352 and H4 hyperacetylation are drastically and specifically reduced in *Dot1l*-KO elongating spermatids.
353 Several acetyltransferases are involved in H4 hyperacetylation such as KAT2A, CBP-P300 or NuA4

354 complex (Boussouar *et al*, 2014; Luense *et al.*, 2019; Shiota *et al.*, 2018) but none of them was found
355 deregulated in *Dot1l*-KO spermatids. We therefore propose that the decrease in histone acetylation is
356 a consequence of impaired H3K79 methylation. In other contexts than the male germline, H4
357 acetylation and H3K79 methylation have previously been shown to influence each other in different
358 ways. In 2016, Gilan *et al.* proposed that DOT1L-mediated H3K79me2 leads to a more open chromatin
359 which facilitates the recruitment of the histone acetyltransferase P300 which, in turn, increases
360 histone H4 acetylation (in particular of H4K5ac), in a cell model of acute myeloid leukemia (Gilan *et al*,
361 2016). In contrast, H4K16ac has been shown to stabilize the binding of yeast Dot1 and human DOT1L
362 on the nucleosome and consequently stimulates its methyltransferase activity *in vitro* (Valencia-
363 Sanchez *et al*, 2021). In elongating spermatids, H3K79 methylation and H4 acetylation could therefore
364 contribute to increase each other signal. It would be interesting to test if H3K79 methylation level is
365 affected in spermatids in which histone acetylation is impaired, for instance in *Kat2a* knockout
366 spermatids.

367 In our study, we also observed a decrease in the three methylation states of H4K20 in elongating
368 spermatids. This is in line with the observation made by Jones et al. (Jones, Su et al., 2008) that H4K20
369 tri-methylation level is reduced at centromeres and telomeres of *Dot1l*-KO embryonic stem cells. H3K9
370 di-methylation (but not tri-methylation) was also found reduced in KO embryonic stem cells, but this
371 histone PTM could not be detected in our analyses. Methylation of H4K20 has been shown to be
372 associated with chromatin accessibility. H4K20me1, by changing the conformation of nucleosomes,
373 increases accessibility for other factors involved in DNA processing and expression (Shoaib *et al*, 2021).
374 In contrast, H4K20me2 and H4K20me3 are associated with chromatin compaction (Evertts *et al*, 2013).
375 For the moment, the impact of these marks during spermatid differentiation is unknown, but
376 H4K20me3 is one of the most dynamic histone modifications during spermatogenesis, with a peak in
377 elongating spermatids ; H4K20me2 follows the same pattern but is less abundant than H4K20me3
378 (Luense *et al.*, 2016; Wang *et al*, 2021). One can therefore speculate that H4K20 methylation is also
379 important for histone to protamine transition. Interestingly, Ho *et al*. have found that the H4K20me1
380 methyltransferase, SET8, and DOT1L (which is a non-SET domain methyl-transferase) bind to the
381 nucleosomal acidic patch by a similar mechanism (Ho *et al*, 2021). Further work will be needed to
382 understand the mechanism by which DOTL1 and/or H3K79 methylation may influence H4K20
383 methylation.
384 Other, more modest quantitative changes in histone PTMs and variants were observed in elongating
385 spermatids. They could be compensatory mechanisms for H3K79 methylation or H4 acetylation
386 decrease, as observed in *Th2b* knock-out spermatids where H2B was upregulated and several histone
387 PTMs changed to compensate for the loss of H2B variant TH2B (Montellier *et al.*, 2013). The

388 deregulation of genes associated to "chromatin function" could also contribute to the changes in
389 chromatin content observed in *Dot1l*-KO spermatids.
390
391 In conclusion, our data show that DOT1L is indispensable for the differentiation of postmeiotic germ
392 cells into functional spermatozoa. Indeed, DOT1L regulates the expression of genes essential for
393 spermatid differentiation and, DOT1L-mediated H3K79 methylation is necessary for proper histone H4
394 hyperacetylation in elongating spermatids and for an efficient histone-to-protamine transition and
395 subsequent compaction of the sperm chromatin.

396

397 # Materials and methods
398

399 **Mouse strains and genotyping**

400 Conditional *Dot1l* knockout mice were obtained from the Knockout Mouse Project (CSD29070) (to
401 F.V.D). This line has previously been described in (Jo *et al.*, 2011). In these mice, *Dot1l* exon 2 is flanked
402 by loxP sites (see Appendix FigS1D). Recombination of loxP sites by Cre recombinase leads to the
403 deletion of exon 2 and consequently a frameshift and premature stop codon in *Dot1l* Coding DNA
404 sequence. Tg(*Stra8-iCre*)1Reb/J were obtained from the Jackson lab (JAX stock #017490) (Sadate-
405 Ngatchou *et al.*, 2008). All animals analyzed in this study were from a C57BL6/J background. Genotypes
406 of animals were determined by polymerase chain reaction (PCR) using *Dot1l* primers F+R1+R2
407 (Appendix FigS1D) or *iCre* primers as described on the Jackson lab website. The latter PCR was
408 performed with *Ymtx* internal control (see Appendix Table S1 for primer list and sequences).
409 Unless specified, all experiments were performed on (adult) 3 to 5 month-old males. Reproductive
410 parameters were analyzed on two types of *Dot1l* knocked-out animal models. First, on animals hosted
411 in a conventional animal house (cah) and of the following genotypes: *Dot1l*$^{Fl/Fl}$; *Stra8-Cre* mice
412 (DOT1Lcah) and *Dot1l*$^{Fl/Fl}$ siblings (without *Stra8*-Cre transgene) as controls (CTLcah). Second, on
413 animals hosted in a Specific Pathogen-Free (SPF) animal house and of the following genotypes: *Dot1l*$^{Fl/\Delta}$
414 *; Stra8-Cre* (hereafter called DOT1L-KO) and *Dot1l*$^{Fl/Fl}$ siblings as controls (hereafter called CTL).
415 Analyses of the reproductive parameters of both types of KO males (*Dot1l*$^{Fl/Fl}$;*Stra8-Cre* or *Dot1l*$^{Fl/\Delta}$*;*
416 *Stra8-Cre*) gave similar results (Appendix FigS2A and B). Heterozygous *Dot1l*$^{Fl/\Delta}$ males (HET) were also
417 analyzed. They did not differ from controls (Appendix FigS2A-E). *Dot1l*$^{Fl/\Delta}$*; Stra8-Cre* animals were
418 generated because it had been shown that *Stra8-iCre* is not 100 % efficient (Bao *et al.*, 2013). In these
419 animals, one allele of *Dot1l* is floxed and one allele is already deleted (Δ) to increase the efficiency of
420 floxed exon excision upon *Cre* recombinase expression. Nevertheless, some remaining DOTL1 protein

421 signal was observed by Western blot and Immunofluorescence (see Figs 1B, D and Appendix FigS1E-I).
422 All other phenotypic analyses and all molecular analyses were performed on *Dot1l*$^{Fl/\Delta}$ *; Stra8-Cre,*
423 hereafter called *Dot1l*-KO, and on *Dot1l*$^{Fl/Fl}$ siblings as CTL. Mice from mTmG line (Muzumdar *et al*,
424 2007) were crossed to *Stra8-Cre* line to verify *Stra8-Cre* recombinase location and activity**.**

425 The mice were fed ad libitum with a standard diet and maintained in a temperature- and light-
426 controlled room. Animal procedures were approved by Universite de Paris ethical committee (Comite
427 d'Ethique pour l'Experimentation Animale; registration number CEEA34.JC.114.12, APAFIS 14214-
428 2017072510448522v26).

429 **Fertility tests**

430 *Dot1l*-KO and CTL males, aged from 8 to 10 weeks, were housed with two wild-type C57BL6/J females
431 per cage (aged from 6 weeks, Janvier Labs, France) for up to 4 months. Vaginal plugs were checked and
432 females separated when found. For each group, litter size and number were assessed.

433 Another series of test were performed too evaluate the fertilization rate following mating (in vivo
434 fertilization). For this WT females were first superovulated by injection of 5 IU of PMSG (pregnant
435 mare's serum gonadotrophin; Intervet, France) followed by 5 IU of hCG (human chorionic
436 gonadotrophin; Intervet) 48 h later. Females were then mated with WT or *Dot1l*-KO males at night and
437 the next day females with a vaginal plug were isolated. Oocytes were collected from ampullae of
438 oviducts and freed from the cumulus cells by brief incubation at 37°C with hyaluronidase (Sigma, St.
439 Louis, MO, USA) in M2 medium (Sigma). Oocytes were rinsed and the number of fertilized oocytes was
440 evaluated using DAPI immune-fluorescent staining to visualize the DNA.

441 **IVF**

442 Oocyte preparation: WT C57BL6/J female mice aged 6 to 8 weeks (Janvier Labs, France) were
443 superovulated with 5 IU of pregnant mare serum gonadotropin (PMSG) and 5 IU human chorionic
444 gonadotropin (hCG) (Intervet, France) 48 hours apart. About 14 hours after hCG injection, animals
445 were sacrificed by cervical dislocation. Cumulus oocyte complexes were collected by tearing the
446 ampulla wall of the oviduct, placed in Ferticult medium (FertiPro N.V, Belgium) supplemented with 3
447 % BSA (Sigma–Aldrich), and maintained at 37°C under 5 % CO2 in air under mineral oil (FertiPro N.V,
448 Belgium). When experiments were performed with Zona-free oocytes, cumulus cells were first
449 removed by a brief exposure to hyaluronidase IV-S (1 mg/ml, Sigma–Aldrich). The zona pellucida was
450 then dissolved with acidic Tyrode's (AT) solution (pH 2.5) (Sigma–Aldrich) under visual monitoring.
451 Zona-free eggs were rapidly washed five times and kept at 37°C under 5 % CO2 in air for 2 to 3 hours
452 to recover their fertilization ability.

453 Capacitated sperm preparation: mouse spermatozoa were obtained from the cauda epididymides of
454 DOT1L-KO, CTL, HET and WT C57BL6/J males (aged 8 to 12 weeks) and capacitated at 37°C under 5 %
455 CO2 for 90 minutes in a 500 µl drop of Ferticult medium supplemented with 3 % BSA, under mineral
456 oil.

457 *In vitro* fertilization: cumulus-intact and Zona-free eggs were inseminated with capacitated
458 spermatozoa for 3 hours in a 100 µl drop of Ferticult medium, 3 % BSA at a final concentration of 10^6
459 or 10^5 per ml, respectively. Then, they were washed and directly mounted in Vectashield/DAPI (Vector
460 laboratories, CA, USA) for observation under UV light (Nikon Eclipse E600 microscope). Only oocytes
461 showing at least one fluorescent decondensed sperm head within their cytoplasm were considered
462 fertilized.

463 **Testicular germ cell purification by elutriation or FACS**

464 Germ cells were purified from adult males using fluorescence-activated cell sorting (FACS) or
465 elutriation as previously described in (Cocquet *et al*, 2009; Comptour *et al*, 2014) and more recently in
466 (Crespo *et al*, 2020). Elutriated fractions with a purity ∼95–99% for elongating/condensing spermatids
467 and ~80% for round spermatids, were used for LC-MS/MS analyses. Highly enriched fractions of
468 primary or secondary spermatocytes (>90%) and round spermatids (∼99%) were used for RNA-Seq
469 analyses. Flow cytometric analysis of testicular cell suspension were performed as previously described
470 (Corbineau *et al*, 2017; Ragazzini *et al*, 2019).

471 **Sperm collection and purification with Percoll**

472 Spermatozoa were extracted from cauda epididymis in pre-warmed (37°C) M2 medium (Sigma-Aldrich)
473 by gentle pressure. Then, epididymides were perforated with a thin needle and incubated in M2 for
474 10 min at 37°C to allow remaining sperm to swim up. For molecular analyses, spermatozoa were next
475 purified on a Percoll gradient. In brief, spermatozoa were centrifuged at 2000 g for 10 min and pellets
476 incubated in somatic cell lysis buffer (1X PBS, 0.1% SDS, 0.5% Triton X-100) for 10 min on ice. Sperm
477 cells were washed with PBS-BSA (1X PBS, 0.5% BSA, 2mM EDTA) and briefly sonicated to remove
478 flagella (ON 5 sec – OFF 30 sec x 3 Cycles, bioruptor Pico, Diagenode). The samples were transferred in
479 low retention tubes, loaded on 50% Percoll (Sigma-Aldrich) and centrifuged at 2500 g for 5 min to
480 remove somatic cells and flagella. This step was repeated once and sperm cells were washed in PBS-
481 BSA twice and counted (minimum 1 000 cells). The purity was >99.7%. Spermhead pellets were snap-
482 frozen in liquid nitrogen and stored at -80°C prior to use.

483 **Nucleoplasmin decompaction**

484 Experiments were performed as previously described in (Yamaguchi *et al*, 2018). Following Percoll
485 purification, sperm heads were washed in 1X PBS, 0.5% Tween, permeabilized with 0.02 U/M
486 Streptolysin O (Sigma-Aldrich) in 1X PBS for 10 min on ice and washed once with 1X PBS, 0.5% Tween.
487 Cells were then incubated with 1X PBS containing 1 mM DTT for 10 min at 37°C, washed with 1X PBS,
488 0.5% Tween, resuspended in KH buffer (100 mM KCl, 20 mM Hepes-KOH, pH 7.7) in low retention tubes
489 and stored at -80°C for later use. Ten million of sperm heads were resuspended in 1 mL NPM treatment
490 buffer (20 mM HEPES-KOH, pH 7.7, 100 mM KCl, 2.5 mM MgCl2, 5 mM Na-But, 10 mM DTT,
491 1X complete EDTA-free protease inhibitors, 250 µM NPM) and incubated for 2 h at 37 °C in a
492 Thermomixer (Mixer HC, Starlab) at 1000 rpm. After centrifugation at 20 000 g for 5 min at 4°C, cells
493 were washed with 5 mM Na-But in 1X PBS, 0.5% Tween twice and sperm heads were fixed with 1%
494 PFA for 10 min at RT, quenched with 250 mM glycine and washed in 5 mM Na-But in PBS/Tween 0.5%
495 twice.

496 After fixation, sperm pellets were resuspended in NP40 Buffer (10 mM Tris-HCl, pH 8.0, 10 mM NaCl,
497 0.5% NP40, 1X complete EDTA-free protease inhibitors, Sigma Aldrich) and incubated on ice for 30 min.
498 Samples were washed with 1X PBS, 0.5% Tween, 5 mM Na-But, and resuspended in 200 µL of
499 sonication buffer (10 mM Tris-HCl, pH 8.0, 20% glycerol, 0.25% SDS, 5 mM Na-But, 1X complete EDTA-
500 free protease inhibitors). Sperm cells were sonicated (ON 30sec – OFF 30sec x13 cycles, Bioruptor Pico,
501 Diagenode) and the sheared chromatin was centrifuged at 20 000 x g for 10 min at 4°C. Supernatants
502 were transferred in new 1.5 mL tubes and pellets resuspended in 200 µL of KH buffer. Prior to western-
503 Blot analyses, both supernatant and pellets were resuspended in 4X NuPage/10% β-mercapto-ethanol
504 (ThermoFisher), heated 10 min at 95°C and briefly sonicated.

505 **Histone extraction from spermatozoa**

506 Experiments were performed as described in (Crespo *et al.*, 2020) with minor modifications. In brief,
507 five million of Percoll-purified and sonicated spermheads were incubated in 50mM DTT for 30 min (at
508 4°C) then mixed with sulfuric acid (0.4M final volume), sonicated and acid extracted with 20%
509 trichloroacetic acid (TCA). Histone pellets were washed with cold acetone containing 0.05% HCl, dried
510 at room temperature, and resuspended in 50µl of SDS-PAGE loading buffer containing 10% β-
511 mercapto-ethanol.

512 **Western blot**

513 Electrophoresis was performed in polyacrylamide gels at 120 V in denaturating buffer containing 25
514 mM Tris Base, 190 mM glycine, 0.1 % SDS and proteins were transferred on nitrocellulose membranes
515 (GE Healthcare). Membranes were then rinsed and incubated 3 min in Ponceau stain to visualize
516 transfer efficiency. Then membranes were incubated in 1X PBS, 0.01 % Tween, 5 % milk. All primary

517 antibodies were incubated over night at 4°C (see Appendix Table S2 for references and dilutions) and
518 2 h at room temperature for secondary antibodies. The revelation was performed with SuperSignal
519 West Pico Plus® ECL from ThermoFisher (34580) and Immobilon ECL Ultra Western HRP substrate from
520 Millipore (WBULS0100) on ImageQuant™ LAS 4000 imager.

521 **Extraction and analysis of protamines**

522 PRM1/PRM2 protamine ratio was analyzed following procedures of protamine-rich fraction of sperm
523 nuclear proteins extraction and analysis previously described, with minor modifications (Soler-Ventura
524 *et al*, 2018). Briefly, histones and other basic proteins loosely attached to DNA were extracted
525 incubating sperm in 0.5 M HCl for 10 min at 37 ºC after vortexing, and centrifuged at 2000 *g* 20 min at
526 4 ºC. This step was repeated three times. Resulting pellet was resuspended in 0.5 % Triton X-100, 20
527 mM Tris-HCl (pH 8), and 2 mM $MgCl_2$. After centrifugation at 8940 *g* 5 min at 4 ºC, the sediment was
528 resuspsended in milliQ H_2O with 1 mM PMSF, centrifuging again at the same conditions. Chromatin
529 was then denaturated by resuspending the pellets in 20mM EDTA, 1mM PMSF, 100mM Tris-HCl- pH8)
530 and adding 1 volume of 575 mM DTT in 6 M GuHCl prior vortexing. The solution was incubated at 37
531 ºC with 0.8 % 4-vynilpyridine to inhibit cysteine disulfide bonds for 30 min, vortexing every 5 min, in
532 fumehood and in dark conditions. Chromatin was then precipitated with a minimum of 10 min
533 incubation with cold ethanol at -20 ºC, followed by centrifugation 12880 *g* for 15 min at 4 ºC. Basic
534 nuclear proteins (protamine-enriched fraction) were extracted from DNA incubating with 0.5 M HCl at
535 37 ºC and recovered in the supernatant after centrifugation at 17530 *g* for 10 min at 4 ºC. Precipitation
536 was carried out with 20 % TCA on ice and centrifugation using the same conditions. Protamines were
537 washed twice with 1 % β-mercaptoethanol in acetone and dried out at room temperature. For in-gel
538 quantification, dried purified extracts were resuspended 5.5 M urea, 20% β-mercaptoethanol, 5%
539 acetic acid, and separated using acetic-acid urea gel electrophoresis (AU-PAGE). Gels were stained with
540 EZBlue™ Gel Staining Reagent (#G1041, Sigma Aldrich) and optic density of the bands corresponding
541 to mouse PRM1 and PRM2 was quantified using Quantity One 1-D analysis software (BioRad, Hercules,
542 CA, USA) to calculate the PRM1/PRM2 ratio. PRM1/PRM2 ratios were normalized against the mean
543 value of the control group.

544 For western blot detection, basic nuclear protein extracts from 2.1M spermatozoa were loaded into
545 AU-PAGE. Proteins were then transferred towards the negative pole onto a 0.45µm pore size
546 nitrocellulose membrane (88018, ThermoFisher) for 4h at 4°C using an acidic transfer buffer consisting
547 of 0.9mM acetic acid. The rest of the procedure (blocking, antibody incubation and ECL detection) was
548 similar as for other western blot experiment (see dedicated paragraph above).

549 **Histological analyses**

550 Mouse testes were fixed in 4 % buffered paraformaldehyde (PFA) for minimum 4 h, before they were
551 cut in halves and incubated overnight in Bouin (Sigma). Testes were then washed in 70 % ethanol at
552 room temperature for 30 min, dehydrated, and embedded in paraffin. Four µm-sections were stained
553 with periodic acid–Schiff (PAS).

554 **Immunohistochemistry and immunofluorescence**

555 Mouse testes were fixed in 4 % buffered paraformaldehyde (PFA) for minimum 4 h, before they were
556 cut in halves and incubated overnight in 4 % PFA. Testes were then washed in 70 % ethanol at room
557 temperature for 30 min, dehydrated, and embedded in paraffin. Immunohistochemistry or
558 immunofluorescence experiments were performed on 4 µm-sections using Novolink polymer
559 detection system (7140-K, Leica Micro-systems) according to the manufacturer's instructions, or
560 following the procedure described in (Comptour *et al.*, 2014) with the following modifications.
561 Permeabilization was performed for 15 min in 1X PBS, 0.5 % Triton X-100. Blocking was performed for
562 30 min to 1 h at room temperature in 1X PBS, 0.1 % Tween, 1 % BSA. Primary antibody was incubated
563 overnight at 4°C (dilution and reference of each antibody are available in Appendix Table S2). Some
564 slides were counterstained with Hematoxylin. For immunofluorescence experiments, lectin (L-21409
565 or L-32459, ThermoFisher) was diluted at 1/500 in 1X PBS and incubated for 1 h at room temperature
566 along with secondary antibodies (see (Comptour *et al.*, 2014)). Lectin was used to stain the developing
567 acrosome and determine the stage of testis tubules as described in (Ahmed & de Rooij, 2009). DAPI (in
568 VECTASHIELD Mounting Medium, Vectorlab) was used to stain nuclei. TUNEL assay was performed on
569 4 µm paraffin-embedded testicular sections using In Situ Cell Death Detection Kit, Fluorescein as
570 described by the manufacturer (Roche, Sigma-Aldrich). GFP immunofluorescence pictures were taken
571 with a NikonE600 microscope using the Nikon Digital Sight SD-V3 camera (DS-Fi1) with the NIS
572 software. All other immunofluorescence pictures were taken with an Olympus BX63 microscope and
573 analysed using ImageJ 1.48v (http://imagej.nih.gov/ij/). Immunohistochemistry pictures were taken
574 with Perkin Elmer Lamina slide scanner and analyzed using CaseViewer software.

575 **Papanicolaou staining of spermatozoa**

576 Spermatozoa were collected from cauda epididymides in M2 medium (Sigma-Aldrich) and spread onto
577 a Superfrost Plus slide (ThermoFisher). Cells were fixed in 4 % PFA for 10 min and stained using
578 Papanicolaou staining. Briefly, the slides were washed in 95 % ethanol, incubated in Harris hematoxylin
579 for 3 min for nucleus counterstaining, washed and stained with OG-6 dye (RAL diagnostics 05.12013,
580 Martillac, France) and with EA-50 (RAL diagnostics 05.12019, Martillac, France). The slides were then
581 dehydrated and mounted with permanent mounting medium. Spermatozoa were then observed with
582 NikonE600 optic microscope and pictures were taken with the 40X objective.

583 **Electron microscopy**

584 Ten to 20 million epidydimal spermatozoa were collected in 2ml of fresh M2 medium (Sigma-Aldrich)
585 prewarmed at 37°C. After pelleting the sperm at room temperature (300g, 10 min), the pellet was fixed
586 in 3 % glutaraldehyde for 1 h before washing twice in 1X PBS (1000g, 10 min). Samples were then
587 dehydrated in ethanol baths and incubated in propylene oxide before inclusion in gelatin. Slices of 60
588 nm were cut with a Diatome and observed with a *JEOL 1011* microscope at a magnification of 1500X
589 or 2000X.

590 **Computer assisted sperm motility analysis (CASA)**

591 Immediately after collection of epididymal spermatozoa in M2 medium (Sigma-Aldrich), sperm motility
592 was analyzed by computer-assisted sperm analysis (CASA) systems CASA CEROS II (Hamilton Thorne,
593 Beverly, MA, USA), using a Zeiss microscope.

594 **Sample preparation for RNA-Seq**

595 Total RNA from 150,000 to 600,000 cells of sorted primary spermatocytes (SCI), secondary
596 spermatocytes (SCII) and round spermatids (RS) was extracted using the Ambion RNAqueous micro kit
597 (ThermoFisher) following manufacturers' instructions. For each cell type, 5 replicates were analyzed.
598 Quantity and quality were assessed using Bioanalyzer chips (ThermoFisher). Libraries were prepared
599 using the NEBNext Ultra II Directional RNA Library Prep Kit (New England Biolabs) according to supplier
600 recommendations. Paired-end sequencing of 100-bp reads was then carried out on the Illumina
601 HiSeq4000 system.

602 **RNA-Seq analyses**

603 Snakemake was used for RNA-seq analyses (Koster & Rahmann, 2018)(v. 3.9.0). Adaptors were
604 trimmed and reads with poor quality (quality < 20) were filtered out with BBduk from BBTools (v. 38.23,
605 https://sourceforge.net/projects/bbmap/). Alignment was performed on the mouse genome build
606 mm10 (GRCm38.p6) using STAR (Dobin & Gingeras, 2015) (v. 2.7.2d) and Gencode vM19 gene
607 annotation GTF with following arguments : --outMultimapperOrder Random --quantMode Genecounts
608 --sjdbOverhang 74. For each sample, the number of aligned reads was converted in cpm (count per
609 million). Genes with an expression level of at least > 1cpm in a minimum of 2 samples were included
610 in the analysis, to exclude genes with a very low expression. Differential expression analysis was carried
611 out using DESeq2 (Love *et al*, 2014) and edgeR (Robinson *et al*, 2010) packages using default
612 parameters and a design using genotype and cell type. Differentially expressed genes (FDR<5%) were
613 obtained using glmTreat edgeR's function which conducts a modified likelihood ratio test (LRT) against
614 the fold change threshold (> 1.5). This method is based on TREAT method (McCarthy & Smyth, 2009).

615 Two analyses were performed in parallel: one selecting the deregulated genes with a FDR < 5%
616 (adjusted p-values), and one selecting deregulated genes with a p-value < 5% (non-adjusted p-values).
617 On this second category of genes, the FDR was calculated *a posteriori* using Benjamini-Hochberg
618 correction (Benjamini & Hochberg, 1995) and was confirmed to be < 5%. Enrichment analysis was
619 performed with GSEA (v. 4.0.3, c5.all.v7.1.symbols.gmt, GO cellular components, biological pathways,
620 or all) on gene expression cpm values between KO and control samples (Subramanian *et al*, 2005) (Fig.
621 S5E). Beforehand, mouse Ensembl gene ID were converted to human Ensembl gene ID (hg38) with the
622 biomaRt R package (Durinck *et al*, 2005). The search for DNA motif in the promoter regions of
623 deregulated genes was performed using HOMER (Heinz *et al*, 2010) with the findMotifs.pl function and
624 the following parameters: -start -2000 -end 0.

625 To generate Appendix FigS1B, we used https://rgv.genouest.org/ (Darde *et al*, 2019; Darde *et al*, 2015).

626 **ChIP-Seq analyses**

627 Snakemake was used for ChIP-Seq analyses. Adaptor were trimmed and filtered using the same
628 parameters than RNA-Seq analyses. Alignment was performed on the mouse genome (mm10) using
629 bowtie2 (Langmead & Salzberg, 2012) with the following arguments: --local. Peak calling was process
630 with MACS2 (Zhang *et al*, 2008) with default parameters against input file to obtains peaks enrichment
631 score of H3K79me2. Mitochondrial peaks and peaks with FDR > 5% were filtered. Peaks were
632 annotated with the R package ChIPseeker (Yu *et al*, 2015) using the annotatePeak() function with the
633 following parameters tssRegion = c(-3000,3000).

634 **Code availability**

635 The fully reproducible and documented analysis for RNA-Seq and ChIP-Seq is available on github at
636 https://github.com/ManonCoulee/RNAseq_DOT1L_Blanco_2022.

637 **MS quantification of histone PTMs and of histone variants**

638 To identify histone PTMs, samples were prepared and processed essentially as described in Crespo *et*
639 *al.* (Crespo *et al.*, 2020). Briefly, histones were precipitated by acid extraction from whole testes which
640 were beforehand reduced into powder using a pestle and mortar on dry ice, or from elutriated
641 elongating/condensing spermatids (ES). They were resuspended in loading gel buffer (LDS sample
642 buffer reference 84788, supplemented with NuPAGE sample reducing agent reference NP0009,
643 ThermoFisher) and separated on a 4-12% NuPAGE acrylamide gel (reference NP0321BOX,
644 ThermoFisher). After blue staining (SimplyBlue SafeStain, ThermoFisher), gel bands corresponding to
645 H3 (at about 17 kDa) and H4 (at about 14 kDa) and two gel slices in-between containing H2A and H2B,
646 were cut and then reduced with dithiothreitol, alkylated with iodoacetamide and in-gel digested with

647 0.1 µg trypsin (V511, Promega) per slice using a Freedom EVO150 robotic platform (Tecan Traging AG,
648 Switzerland). Alternatively, to analyze the relative abundance of histone variants between conditions,
649 histone samples were simply loaded on a gel and migrated for a few mm. The whole zone was cut for
650 robotic in-gel tryptic digestion. The resulting tryptic peptides were analyzed by a liquid
651 chromatography-tandem mass spectrometry coupling made up of a C18 reversed-phase capillary
652 column (75 µm i.d. x 25 cm ReproSil-Pur C18-AQ, 1.9 µm particles, Cluzeau, France) using the
653 UltiMate™ 3000 RSLCnano system (ThermoFisher) coupled to a Q-Exactive HF mass spectrometer
654 (ThermoFisher). The mobile phases consisted of water with 0.1% formic acid (A) and acetonitrile with
655 0.08% (v/v) formic acid (B). Peptides were eluted with a gradient consisting of an increase of solvent B
656 from 2.8% to 7.5% for 7.5 min, then from 7.5% to 33.2% over 33.5 min and finally from 33.2% to 48%
657 over 6.5 min. Mass spectrometry acquisitions were carried out by alternating one full MS scan with
658 Orbitrap detection acquired over the mass range 300 to 1300 m/z and data-dependent MS/MS spectra
659 on the 10 most abundant precursor ions detected in MS. The peptides were isolated for fragmentation
660 by higher-energy collisional dissociation (HCD) with a collision energy of 27.

661 Identification of modified peptides was obtained using our in-house established database of histone
662 sequences, MS_histoneDB (El Kennani *et al*, 2017), completed with a list of 500 common contaminants.
663 MS/MS data interpretation was carried out with the program Mascot
664 (http://www.matrixscience.com/) with the following search parameters. The precursor and fragment
665 mass tolerances were 5 ppm and 25 mmu, respectively; enzyme specificity was trypsin; the maximum
666 number of trypsin missed cleavages was set to 5, carbamidomethyl (Cys) was specified as a fixed
667 modification. We indicated as variable PTMs in Mascot acetylation, crotonylation and ubiquitination
668 (more precisely the dipeptide "GlyGly") of Lys residues, methylation and di-methylation of Lys/Arg and
669 tri-methylation of Lys, as well as N-terminal acetylation of proteins. Filtering of peptide identifications
670 and quantification was performed by using the program Proline (Bouyssie *et al*, 2020). All
671 peptide/spectrum matches of scores below 15 were filtered out; next, all identifications of modified
672 peptides suggested by Mascot for H3 and H4 were visually validated by demanding that a continuous
673 stretch of minimally 5 amino acids be identified in terms of b or y fragment ions, and by ascertaining
674 PTM positioning on Lys/Arg residues. This score threshold is very low, yet it was relevant to use so as
675 to be able to identify very short peptides, such as H3-K18modQLATK. When interpreting our mass
676 spectrometry data against the database MS_histoneDB, we were able to identify and quantify various
677 H3 variants, namely canonical H3 and variants H3.3, testis-specific H3t and H3mm13. H3t differs from
678 canonical H3 at residue 24, while H3.3 and H3mm13 differ from H3 at residues 31 and 29. To estimate
679 the relative abundance of modified histone peptides between samples, normalization to be at constant
680 amount of total H2A, H2B, H3 or H4 was done by dividing the raw MS signals of modified peptides by

681 the sum of the MS signals of modified and unmodified peptides for each histone. To estimate the
682 relative abundance of histone variants between *Dot1l*-KO and CTL samples, variants were quantified
683 by Proline by relying only on peptides specific of these sequences. Samples were normalized to be at
684 constant amount of histone H4. The mass spectrometry proteomics data have been deposited to the
685 ProteomeXchange Consortium via the PRIDE (Perez-Riverol *et al*, 2019) partner repository with the
686 dataset identifier PXD030734 and 10.6019/PXD030734.

687 **Statistical Analysis**

688 Chi-square and unpaired t-test were used to analyze IVF data. Sperm motility parameters were
689 analyzed using a Mann Whitney tests following angular transformation of percentages. To compare
690 the incidence of sperm head abnormalities, and apoptotic (TUNEL+) spermatids between *Dot1l*-KO and
691 CTL, percentages were converted in angles prior to performing t-tests. Student t-test (corrected for
692 multiple testing when appropriate) was used for all other analyses (fertility, sperm count, testis weight,
693 histology, histone PTM, western blot, and normalized PRM1/2 ratio quantifications). Statistical
694 analyses for RNA-Seq/ChIP-Seq are described in the dedicated paragraphs.

695

696 Data availability

697 RNA-Seq data have been submitted to ENA repository under project number PRJEB50887
698 (https://www.ebi.ac.uk/ena/). H3K79me2 ChIP-Seq project number is PRJNA643726. The mass
699 spectrometry proteomics data have been deposited to the ProteomeXchange Consortium via the
700 PRIDE (Perez-Riverol et al., 2019) partner repository with the dataset identifier PXD030734 and
701 10.6019/PXD030734.

702

703 Acknowledgements

704 We would like to thank Cochin Institute (INSERM U1016, CNRS UMR8104, Universite Paris Cité) core
705 facilities, in particular, Alain Schmitt from the electron microscopy platform, and all the staff from the
706 animal house, histology (HistIM), genomic (GENOM'IC), cytometry (CYBIO) and imaging (IMAG'IC) core
707 facilities. We would also like to thank Guillaume Meurice for advices on bioinformatics analyses, and
708 Aminata Touré and Marjorie Whitfield for advices and discussion on sperm morphology and motility
709 analyses. M.Cr. and D.P. are grateful to their colleagues in EDyP for their support on LC-MS instruments
710 and in informatics. This work was supported by the Agence Nationale de la Recherche (ANR-17-CE12-
711 0004-01 to J.C., ANR-21-CE44-0035 to D.P.), the Fondation pour la Recherche Médicale

(SPF201909009274 to C.G.) and grants from “Ministerio de Economía y competitividad” FI17/00224 to A.I., and “Ministerio de Ciencia e Innovación” PI20/00936 to R.O. and MV20/00026 to A.I. M.B and M.Co. received a PhD funding from Université Paris Cité, M. Cr., from University Grenoble Alps (UGA). The proteomic experiments were partially supported by Agence Nationale de la Recherche under projects ProFI (Proteomics French Infrastructure, ANR-10-INBS-08) and GRAL, a program from the Chemistry Biology Health (CBH) Graduate School of University Grenoble Alpes (ANR-17-EURE-0003).

Disclosure and Competing Interests Statement

The authors declare that they have no conflict of interest.

References

Aguilar D, Strom J, Chen QM (2014) Glucocorticoid induced leucine zipper inhibits apoptosis of cardiomyocytes by doxorubicin. *Toxicol Appl Pharmacol* 276: 55-62

Ahmed EA, de Rooij DG (2009) Staging of mouse seminiferous tubule cross-sections. *Methods Mol Biol* 558: 263-277

Arevalo L, Merges GE, Schneider S, Oben FE, Neumann IS, Schorle H (2022) Loss of the cleaved-protamine 2 domain leads to incomplete histone-to-protamine exchange and infertility in mice. *PLoS Genet* 18: e1010272

Aslam MA, Alemdehy MF, Kwesi-Maliepaard EM, Muhaimin FI, Caganova M, Pardieck IN, van den Brand T, van Welsem T, de Rink I, Song JY *et al* (2021) Histone methyltransferase DOT1L controls state-specific identity during B cell differentiation. *EMBO Rep* 22: e51184

Bao J, Bedford MT (2016) Epigenetic regulation of the histone-to-protamine transition during spermiogenesis. *Reproduction (Cambridge, England)* 151: R55-70

Bao J, Ma HY, Schuster A, Lin YM, Yan W (2013) Incomplete cre-mediated excision leads to phenotypic differences between Stra8-iCre; Mov10l1(lox/lox) and Stra8-iCre; Mov10l1(lox/Delta) mice. *Genesis* 51: 481-490

Barral S, Morozumi Y, Tanaka H, Montellier E, Govin J, de Dieuleveult M, Charbonnier G, Coute Y, Puthier D, Buchou T *et al* (2017) Histone Variant H2A.L.2 Guides Transition Protein-Dependent Protamine Assembly in Male Germ Cells. *Mol Cell* 66: 89-101 e108

Barraud-Lange V, Ialy-Radio C, Chalas C, Holtzmann I, Wolf JP, Barbaux S, Ziyyat A (2020) Partial Sperm beta1 Integrin Subunit Deletion Proves its Involvement in Mouse Gamete Adhesion/Fusion. *Int J Mol Sci* 21

Benjamini Y, Hochberg Y (1995) Controlling the False Discovery Rate: A Practical and Powerful Approach to Multiple Testing. *Journal of the Royal Statistical Society: Series B (Methodological)* 57: 289-300

Boussouar F, Goudarzi A, Buchou T, Shiota H, Barral S, Debernardi A, Guardiola P, Brindle P, Martinez G, Arnoult C *et al* (2014) A specific CBP/p300-dependent gene expression programme drives the metabolic remodelling in late stages of spermatogenesis. *Andrology* 2: 351-359

Bouyssie D, Hesse AM, Mouton-Barbosa E, Rompais M, Macron C, Carapito C, Gonzalez de Peredo A, Coute Y, Dupierris V, Burel A *et al* (2020) Proline: an efficient and user-friendly software suite for large-scale proteomics. *Bioinformatics* 36: 3148-3155

Braun RE (2001) Packaging paternal chromosomes with protamine. *Nature genetics* 28: 10-12

754 Cattaneo P, Hayes MGB, Baumgarten N, Hecker D, Peruzzo S, Aslan GS, Kunderfranco P, Larcher V,
755 Zhang L, Contu R *et al* (2022) DOT1L regulates chamber-specific transcriptional networks during
756 cardiogenesis and mediates postnatal cell cycle withdrawal. *Nature communications* 13: 7444
757 Chang CC, Ye BH, Chaganti RS, Dalla-Favera R (1996) BCL-6, a POZ/zinc-finger protein, is a sequence-
758 specific transcriptional repressor. *Proceedings of the National Academy of Sciences of the United States*
759 *of America* 93: 6947-6952
760 Chen Y, Zheng Y, Gao Y, Lin Z, Yang S, Wang T, Wang Q, Xie N, Hua R, Liu M *et al* (2018) Single-cell RNA-
761 seq uncovers dynamic processes and critical regulators in mouse spermatogenesis. *Cell Res* 28: 879-
762 896
763 Cocquet J, Ellis PJ, Yamauchi Y, Mahadevaiah SK, Affara NA, Ward MA, Burgoyne PS (2009) The
764 multicopy gene Sly represses the sex chromosomes in the male mouse germline after meiosis. *PLoS*
765 *biology* 7: e1000244
766 Comptour A, Moretti C, Serrentino ME, Auer J, Ialy-Radio C, Ward MA, Toure A, Vaiman D, Cocquet J
767 (2014) SSTY proteins co-localize with the post-meiotic sex chromatin and interact with regulators of its
768 expression. *The FEBS journal* 281: 1571-1584
769 Corbineau S, Lassalle B, Givelet M, Souissi-Sarahoui I, Firlej V, Romeo PH, Allemand I, Riou L, Fouchet
770 P (2017) Spermatogonial stem cells and progenitors are refractory to reprogramming to pluripotency
771 by the transcription factors Oct3/4, c-Myc, Sox2 and Klf4. *Oncotarget* 8: 10050-10063
772 Crespo M, Damont A, Blanco M, Lastrucci E, Kennani SE, Ialy-Radio C, Khattabi LE, Terrier S, Louwagie
773 M, Kieffer-Jaquinod S *et al* (2020) Multi-omic analysis of gametogenesis reveals a novel signature at
774 the promoters and distal enhancers of active genes. *Nucleic Acids Res* 48: 4115-4138
775 da Cruz I, Rodriguez-Casuriaga R, Santinaque FF, Farias J, Curti G, Capoano CA, Folle GA, Benavente R,
776 Sotelo-Silveira JR, Geisinger A (2016) Transcriptome analysis of highly purified mouse spermatogenic
777 cell populations: gene expression signatures switch from meiotic-to postmeiotic-related processes at
778 pachytene stage. *BMC genomics* 17: 294
779 Darde TA, Lecluze E, Lardenois A, Stevant I, Alary N, Tuttelmann F, Collin O, Nef S, Jegou B, Rolland AD
780 *et al* (2019) The ReproGenomics Viewer: a multi-omics and cross-species resource compatible with
781 single-cell studies for the reproductive science community. *Bioinformatics* 35: 3133-3139
782 Darde TA, Sallou O, Becker E, Evrard B, Monjeaud C, Le Bras Y, Jegou B, Collin O, Rolland AD, Chalmel
783 F (2015) The ReproGenomics Viewer: an integrative cross-species toolbox for the reproductive science
784 community. *Nucleic Acids Res* 43: W109-116
785 de Mateo S, Gazquez C, Guimera M, Balasch J, Meistrich ML, Ballesca JL, Oliva R (2009) Protamine 2
786 precursors (Pre-P2), protamine 1 to protamine 2 ratio (P1/P2), and assisted reproduction outcome.
787 *Fertil Steril* 91: 715-722
788 Dobin A, Gingeras TR (2015) Mapping RNA-seq Reads with STAR. *Curr Protoc Bioinformatics* 51: 11 14
789 11-19
790 Dong Y, Isono KI, Ohbo K, Endo TA, Ohara O, Maekawa M, Toyama Y, Ito C, Toshimori K, Helin K *et al*
791 (2017) EPC1/TIP60-Mediated Histone Acetylation Facilitates Spermiogenesis in Mice. *Mol Cell Biol* 37
792 Dottermusch-Heidel C, Gartner SM, Tegeder I, Rathke C, Barckmann B, Bartkuhn M, Bhushan S, Steger
793 K, Meinhardt A, Renkawitz-Pohl R (2014a) H3K79 methylation: a new conserved mark that
794 accompanies H4 hyperacetylation prior to histone-to-protamine transition in Drosophila and rat. *Biol*
795 *Open* 3: 444-452
796 Dottermusch-Heidel C, Klaus ES, Gonzalez NH, Bhushan S, Meinhardt A, Bergmann M, Renkawitz-Pohl
797 R, Rathke C, Steger K (2014b) H3K79 methylation directly precedes the histone-to-protamine transition
798 in mammalian spermatids and is sensitive to bacterial infections. *Andrology* 2: 655-665
799 Durinck S, Moreau Y, Kasprzyk A, Davis S, De Moor B, Brazma A, Huber W (2005) BioMart and
800 Bioconductor: a powerful link between biological databases and microarray data analysis.
801 *Bioinformatics* 21: 3439-3440
802 El Kennani S, Adrait A, Shaytan AK, Khochbin S, Bruley C, Panchenko AR, Landsman D, Pflieger D, Govin
803 J (2017) MS_HistoneDB, a manually curated resource for proteomic analysis of human and mouse
804 histones. *Epigenetics Chromatin* 10: 2

805 Ernst C, Eling N, Martinez-Jimenez CP, Marioni JC, Odom DT (2019) Staged developmental mapping
806 and X chromosome transcriptional dynamics during mouse spermatogenesis. *Nature communications*
807 10: 1251
808 Evertts AG, Manning AL, Wang X, Dyson NJ, Garcia BA, Coller HA (2013) H4K20 methylation regulates
809 quiescence and chromatin compaction. *Mol Biol Cell* 24: 3025-3037
810 Frehlick LJ, Eirin-Lopez JM, Ausio J (2007) New insights into the nucleophosmin/nucleoplasmin family
811 of nuclear chaperones. *Bioessays* 29: 49-59
812 Fujihara Y, Murakami M, Inoue N, Satouh Y, Kaseda K, Ikawa M, Okabe M (2010) Sperm equatorial
813 segment protein 1, SPESP1, is required for fully fertile sperm in mouse. *J Cell Sci* 123: 1531-1536
814 Gadadhar S, Alvarez Viar G, Hansen JN, Gong A, Kostarev A, Ialy-Radio C, Leboucher S, Whitfield M,
815 Ziyyat A, Toure A *et al* (2021) Tubulin glycylation controls axonemal dynein activity, flagellar beat, and
816 male fertility. *Science* 371
817 Gaucher J, Boussouar F, Montellier E, Curtet S, Buchou T, Bertrand S, Hery P, Jounier S, Depaux A, Vitte
818 AL *et al* (2012) Bromodomain-dependent stage-specific male genome programming by Brdt. *The EMBO*
819 *journal* 31: 3809-3820
820 Gilan O, Lam EY, Becher I, Lugo D, Cannizzaro E, Joberty G, Ward A, Wiese M, Fong CY, Ftouni S *et al*
821 (2016) Functional interdependence of BRD4 and DOT1L in MLL leukemia. *Nature structural & molecular*
822 *biology* 23: 673-681
823 Goudarzi A, Zhang D, Huang H, Barral S, Kwon OK, Qi S, Tang Z, Buchou T, Vitte AL, He T *et al* (2016)
824 Dynamic Competing Histone H4 K5K8 Acetylation and Butyrylation Are Hallmarks of Highly Active Gene
825 Promoters. *Mol Cell* 62: 169-180
826 Green CD, Ma Q, Manske GL, Shami AN, Zheng X, Marini S, Moritz L, Sultan C, Gurczynski SJ, Moore BB
827 *et al* (2018) A Comprehensive Roadmap of Murine Spermatogenesis Defined by Single-Cell RNA-Seq.
828 *Developmental cell* 46: 651-667 e610
829 Heinz S, Benner C, Spann N, Bertolino E, Lin YC, Laslo P, Cheng JX, Murre C, Singh H, Glass CK (2010)
830 Simple combinations of lineage-determining transcription factors prime cis-regulatory elements
831 required for macrophage and B cell identities. *Mol Cell* 38: 576-589
832 Ho CH, Takizawa Y, Kobayashi W, Arimura Y, Kimura H, Kurumizaka H (2021) Structural basis of
833 nucleosomal histone H4 lysine 20 methylation by SET8 methyltransferase. *Life Sci Alliance* 4
834 Jo SY, Granowicz EM, Maillard I, Thomas D, Hess JL (2011) Requirement for Dot1l in murine postnatal
835 hematopoiesis and leukemogenesis by MLL translocation. *Blood* 117: 4759-4768
836 Jones B, Su H, Bhat A, Lei H, Bajko J, Hevi S, Baltus GA, Kadam S, Zhai H, Valdez R *et al* (2008) The
837 histone H3K79 methyltransferase Dot1L is essential for mammalian development and
838 heterochromatin structure. *PLoS Genet* 4: e1000190
839 Kawano N, Kang W, Yamashita M, Koga Y, Yamazaki T, Hata T, Miyado K, Baba T (2010) Mice lacking
840 two sperm serine proteases, ACR and PRSS21, are subfertile, but the mutant sperm are infertile in
841 vitro. *Biology of reproduction* 83: 359-369
842 Kim W, Choi M, Kim JE (2014) The histone methyltransferase Dot1/DOT1L as a critical regulator of the
843 cell cycle. *Cell Cycle* 13: 726-738
844 Koster J, Rahmann S (2018) Snakemake-a scalable bioinformatics workflow engine. *Bioinformatics* 34:
845 3600
846 Kuang W, Zhang J, Lan Z, Deepak R, Liu C, Ma Z, Cheng L, Zhao X, Meng X, Wang W *et al* (2021) SLC22A14
847 is a mitochondrial riboflavin transporter required for sperm oxidative phosphorylation and male
848 fertility. *Cell reports* 35: 109025
849 Kurosu T, Fukuda T, Miki T, Miura O (2003) BCL6 overexpression prevents increase in reactive oxygen
850 species and inhibits apoptosis induced by chemotherapeutic reagents in B-cell lymphoma cells.
851 *Oncogene* 22: 4459-4468
852 Kwesi-Maliepaard EM, Aslam MA, Alemdehy MF, van den Brand T, McLean C, Vlaming H, van Welsem
853 T, Korthout T, Lancini C, Hendriks S *et al* (2020) The histone methyltransferase DOT1L prevents antigen-
854 independent differentiation and safeguards epigenetic identity of CD8(+) T cells. *Proceedings of the*
855 *National Academy of Sciences of the United States of America* 117: 20706-20716
856 Langmead B, Salzberg SL (2012) Fast gapped-read alignment with Bowtie 2. *Nat Methods* 9: 357-359

857 Lin H, Cheng K, Kubota H, Lan Y, Riedel SS, Kakiuchi K, Sasaki K, Bernt KM, Bartolomei MS, Luo M *et al*
858 (2022) Histone methyltransferase DOT1L is essential for self-renewal of germline stem cells. *Genes &*
859 *development* 36: 752-763
860 Lin YH, Kakadia PM, Chen Y, Li YQ, Deshpande AJ, Buske C, Zhang KL, Zhang Y, Xu GL, Bohlander SK
861 (2009) Global reduction of the epigenetic H3K79 methylation mark and increased chromosomal
862 instability in CALM-AF10-positive leukemias. *Blood* 114: 651-658
863 Love MI, Huber W, Anders S (2014) Moderated estimation of fold change and dispersion for RNA-seq
864 data with DESeq2. *Genome biology* 15: 550
865 Luense LJ, Donahue G, Lin-Shiao E, Rangel R, Weller AH, Bartolomei MS, Berger SL (2019) Gcn5-
866 Mediated Histone Acetylation Governs Nucleosome Dynamics in Spermiogenesis. *Developmental cell*
867 Luense LJ, Wang X, Schon SB, Weller AH, Lin Shiao E, Bryant JM, Bartolomei MS, Coutifaris C, Garcia
868 BA, Berger SL (2016) Comprehensive analysis of histone post-translational modifications in mouse and
869 human male germ cells. *Epigenetics Chromatin* 9: 24
870 Maruyama SY, Ito M, Ikami Y, Okitsu Y, Ito C, Toshimori K, Fujii W, Yogo K (2016) A critical role of solute
871 carrier 22a14 in sperm motility and male fertility in mice. *Sci Rep* 6: 36468
872 McCarthy DJ, Smyth GK (2009) Testing significance relative to a fold-change threshold is a TREAT.
873 *Bioinformatics* 25: 765-771
874 Montellier E, Boussouar F, Rousseaux S, Zhang K, Buchou T, Fenaille F, Shiota H, Debernardi A, Hery P,
875 Curtet S *et al* (2013) Chromatin-to-nucleoprotamine transition is controlled by the histone H2B variant
876 TH2B. *Genes & development* 27: 1680-1692
877 Montellier E, Rousseaux S, Zhao Y, Khochbin S (2011) Histone crotonylation specifically marks the
878 haploid male germ cell gene expression program: Post-meiotic male-specific gene expression.
879 *Bioessays*
880 Moretti C, Serrentino ME, Ialy-Radio C, Delessard M, Soboleva TA, Tores F, Leduc M, Nitschke P, Drevet
881 JR, Tremethick DJ *et al* (2017) SLY regulates genes involved in chromatin remodeling and interacts with
882 TBL1XR1 during sperm differentiation. *Cell death and differentiation* 24: 1029-1044
883 Muzumdar MD, Tasic B, Miyamichi K, Li L, Luo L (2007) A global double-fluorescent Cre reporter mouse.
884 *Genesis* 45: 593-605
885 Nguyen AT, Taranova O, He J, Zhang Y (2011) DOT1L, the H3K79 methyltransferase, is required for MLL-
886 AF9-mediated leukemogenesis. *Blood* 117: 6912-6922
887 Okada Y, Feng Q, Lin Y, Jiang Q, Li Y, Coffield VM, Su L, Xu G, Zhang Y (2005) hDOT1L links histone
888 methylation to leukemogenesis. *Cell* 121: 167-178
889 Oliva R (2006) Protamines and male infertility. *Human reproduction update* 12: 417-435
890 Oliva R, Bazett-Jones D, Mezquita C, Dixon GH (1987) Factors affecting nucleosome disassembly by
891 protamines in vitro. Histone hyperacetylation and chromatin structure, time dependence, and the size
892 of the sperm nuclear proteins. *The Journal of biological chemistry* 262: 17016-17025
893 Onder TT, Kara N, Cherry A, Sinha AU, Zhu N, Bernt KM, Cahan P, Marcarci BO, Unternaehrer J, Gupta
894 PB *et al* (2012) Chromatin-modifying enzymes as modulators of reprogramming. *Nature* 483: 598-602
895 Perez-Riverol Y, Csordas A, Bai J, Bernal-Llinares M, Hewapathirana S, Kundu DJ, Inuganti A, Griss J,
896 Mayer G, Eisenacher M *et al* (2019) The PRIDE database and related tools and resources in 2019:
897 improving support for quantification data. *Nucleic Acids Res* 47: D442-D450
898 Ragazzini R, Perez-Palacios R, Baymaz IH, Diop S, Ancelin K, Zielinski D, Michaud A, Givelet M, Borsos
899 M, Aflaki S *et al* (2019) EZHIP constrains Polycomb Repressive Complex 2 activity in germ cells. *Nature*
900 *communications* 10: 3858
901 Rathke C, Baarends WM, Awe S, Renkawitz-Pohl R (2014) Chromatin dynamics during spermiogenesis.
902 *Biochim Biophys Acta* 1839: 155-168
903 Robinson MD, McCarthy DJ, Smyth GK (2010) edgeR: a Bioconductor package for differential
904 expression analysis of digital gene expression data. *Bioinformatics* 26: 139-140
905 Sadate-Ngatchou PI, Payne CJ, Dearth AT, Braun RE (2008) Cre recombinase activity specific to
906 postnatal, premeiotic male germ cells in transgenic mice. *Genesis* 46: 738-742

907 Shang E, Nickerson HD, Wen D, Wang X, Wolgemuth DJ (2007) The first bromodomain of Brdt, a testis-
908 specific member of the BET sub-family of double-bromodomain-containing proteins, is essential for
909 male germ cell differentiation. *Development (Cambridge, England)* 134: 3507-3515
910 Shiota H, Barral S, Buchou T, Tan M, Coute Y, Charbonnier G, Reynoird N, Boussouar F, Gerard M, Zhu
911 M *et al* (2018) Nut Directs p300-Dependent, Genome-Wide H4 Hyperacetylation in Male Germ Cells.
912 *Cell reports* 24: 3477-3487 e3476
913 Shoaib M, Chen Q, Shi X, Nair N, Prasanna C, Yang R, Walter D, Frederiksen KS, Einarsson H, Svensson
914 JP *et al* (2021) Histone H4 lysine 20 mono-methylation directly facilitates chromatin openness and
915 promotes transcription of housekeeping genes. *Nature communications* 12: 4800
916 Soler-Ventura A, Castillo J, de la Iglesia A, Jodar M, Barrachina F, Ballesca JL, Oliva R (2018) Mammalian
917 Sperm Protamine Extraction and Analysis: A Step-By-Step Detailed Protocol and Brief Review of
918 Protamine Alterations. *Protein Pept Lett* 25: 424-433
919 Soumillon M, Necsulea A, Weier M, Brawand D, Zhang X, Gu H, Barthes P, Kokkinaki M, Nef S, Gnirke
920 A *et al* (2013) Cellular source and mechanisms of high transcriptome complexity in the mammalian
921 testis. *Cell reports* 3: 2179-2190
922 Steger DJ, Lefterova MI, Ying L, Stonestrom AJ, Schupp M, Zhuo D, Vakoc AL, Kim JE, Chen J, Lazar MA
923 *et al* (2008) DOT1L/KMT4 recruitment and H3K79 methylation are ubiquitously coupled with gene
924 transcription in mammalian cells. *Mol Cell Biol* 28: 2825-2839
925 Subramanian A, Tamayo P, Mootha VK, Mukherjee S, Ebert BL, Gillette MA, Paulovich A, Pomeroy SL,
926 Golub TR, Lander ES *et al* (2005) Gene set enrichment analysis: a knowledge-based approach for
927 interpreting genome-wide expression profiles. *Proceedings of the National Academy of Sciences of the*
928 *United States of America* 102: 15545-15550
929 Thomis DC, Lee W, Berg LJ (1997) T cells from Jak3-deficient mice have intact TCR signaling, but
930 increased apoptosis. *J Immunol* 159: 4708-4719
931 Torregrosa N, Dominguez-Fandos D, Camejo MI, Shirley CR, Meistrich ML, Ballesca JL, Oliva R (2006)
932 Protamine 2 precursors, protamine 1/protamine 2 ratio, DNA integrity and other sperm parameters in
933 infertile patients. *Human reproduction (Oxford, England)* 21: 2084-2089
934 Toure A (2019) Importance of SLC26 Transmembrane Anion Exchangers in Sperm Post-testicular
935 Maturation and Fertilization Potential. *Front Cell Dev Biol* 7: 230
936 Valencia-Sanchez MI, De Ioannes P, Wang M, Truong DM, Lee R, Armache JP, Boeke JD, Armache KJ
937 (2021) Regulation of the Dot1 histone H3K79 methyltransferase by histone H4K16 acetylation. *Science*
938 371
939 Vlaming H, van Leeuwen F (2016) The upstreams and downstreams of H3K79 methylation by DOT1L.
940 *Chromosoma*
941 Wang Y, Iwamori T, Kaneko T, Iida H, Iwamori N (2021) Comparative distributions of RSBN1 and
942 methylated histone H4 Lysine 20 in the mouse spermatogenesis. *PloS one* 16: e0253897
943 Wang Z, Zang C, Rosenfeld JA, Schones DE, Barski A, Cuddapah S, Cui K, Roh TY, Peng W, Zhang MQ *et*
944 *al* (2008) Combinatorial patterns of histone acetylations and methylations in the human genome.
945 *Nature genetics* 40: 897-903
946 Ward WS, Coffey DS (1991) DNA packaging and organization in mammalian spermatozoa: comparison
947 with somatic cells. *Biology of reproduction* 44: 569-574
948 Yamaguchi K, Hada M, Fukuda Y, Inoue E, Makino Y, Katou Y, Shirahige K, Okada Y (2018) Re-evaluating
949 the Localization of Sperm-Retained Histones Revealed the Modification-Dependent Accumulation in
950 Specific Genome Regions. *Cell reports* 23: 3920-3932
951 Yamauchi Y, Riel JM, Stoytcheva Z, Burgoyne PS, Ward MA (2010) Deficiency in mouse Y chromosome
952 long arm gene complement is associated with sperm DNA damage. *Genome biology* 11: R66
953 Yu G, Wang LG, He QY (2015) ChIPseeker: an R/Bioconductor package for ChIP peak annotation,
954 comparison and visualization. *Bioinformatics* 31: 2382-2383
955 Yu YE, Zhang Y, Unni E, Shirley CR, Deng JM, Russell LD, Weil MM, Behringer RR, Meistrich ML (2000)
956 Abnormal spermatogenesis and reduced fertility in transition nuclear protein 1-deficient mice.
957 *Proceedings of the National Academy of Sciences of the United States of America* 97: 4683-4688

958 Zhang W, Hayashizaki Y, Kone BC (2004) Structure and regulation of the mDot1 gene, a mouse histone
959 H3 methyltransferase. *The Biochemical journal* 377: 641-651
960 Zhang Y, Liu T, Meyer CA, Eeckhoute J, Johnson DS, Bernstein BE, Nusbaum C, Myers RM, Brown M, Li
961 W *et al* (2008) Model-based analysis of ChIP-Seq (MACS). *Genome biology* 9: R137
962 Zhao M, Shirley CR, Hayashi S, Marcon L, Mohapatra B, Suganuma R, Behringer RR, Boissonneault G,
963 Yanagimachi R, Meistrich ML (2004a) Transition nuclear proteins are required for normal chromatin
964 condensation and functional sperm development. *Genesis* 38: 200-213
965 Zhao M, Shirley CR, Mounsey S, Meistrich ML (2004b) Nucleoprotein transitions during spermiogenesis
966 in mice with transition nuclear protein Tnp1 and Tnp2 mutations. *Biology of reproduction* 71: 1016-
967 1025
968 Zhu B, Chen S, Wang H, Yin C, Han C, Peng C, Liu Z, Wan L, Zhang X, Zhang J *et al* (2018) The protective
969 role of DOT1L in UV-induced melanomagenesis. *Nature communications* 9: 259
970

971

972 ## Figure legends

973 **Figure 1. DOT1L expression in meiotic and postmeiotic germ cells of *Dot1l*-KO and CTL males**

974 A) Spermatogenesis scheme representing the dynamic of histone to protamine transition. B) Western
975 blot detection of DOT1L and TUBULIN (TUB) in whole testicular protein extracts from CTL and *Dot1l*-
976 KO (KO) adult mice. C) Immunohistochemistry detection of DOT1L in testicular sections from CTL and
977 *Dot1l*-KO (KO) adult mice. SC = Spermatocytes, RS = Round spermatids, ES = Elongating spermatids.
978 Pictures were taken using the same parameters. Scale bars indicate 50µm. D) Western blot detection
979 of DOT1L and H3K79me2 in *Dot1l*-KO (KO) and CTL germ cells. Normalization was performed by
980 detecting the membrane with anti-TUBULIN (TUB). SC = primary spermatocytes, RS = round
981 spermatids. See also Fig EV1 and Appendix FigS1.

982 **Figure 2. *Dot1l*-KO in male germ cells impairs spermatogenesis and male fertility**

983 A) Scatter plots (mean + standard deviation) showing the average testis weight, body weight and sperm
984 count in *Dot1l*-KO and CTL adult mice (2 to 4 month-old N>10 for CTL and *Dot1l*-KO samples). B)
985 Histology of *Dot1l*-KO and CTL testes (periodic acid-Schiff staining). Scale bars indicate 200µm. C)
986 Schematic diagram representing total number of each cell type per testis in CTL and *Dot1l*-KO males,
987 as calculated by FACS. 4N = Primary spermatocytes, 2N = Secondary spermatocytes, N = spermatids,
988 SP = Side Population representing premeiotic germ cells (spermatogonia). 8 CTL and 6 *Dot1l*-KO testes
989 were analyzed. One or two stars indicate a p-value <0.05 or <0.01, respectively (Student t-test). D)
990 Results from the tests of fertility (natural mating) of *Dot1l*-KO and CTL males (7 males in each group
991 mated for ~3 months with wild-type females). Schematic diagrams representing the number of litters
992 and the litter size from progeny of *Dot1l*-KO or CTL males (mean + standard deviation). E) In vivo (left
993 panel) and in vitro fertilization results. The percentages of fertilized oocytes are indicated for WT, CTL
994 and HET males ('all CTL') and for *Dot1l*-KO males. The left panel shows the mean fertilization rate (%)

995 of oocytes collected in superovulated females 24h after natural mating). Nine and 6 females with a
996 positive vaginal plug were analyzed after mating with CTL and *Dot1l*-KO males respectively. This
997 represents 113 and 73 oocytes analyzed after mating with CTL or KO males respectively. Two stars
998 indicate a p-value <0.005 (unpaired t-test performed after angular transformation of percentages). The
999 central and right panels show in vitro fertilization results using oocytes with intact cumulus, or using
1000 oocytes of which the zona pellucida was removed beforehand. See also Appendix FigS2.

1001 **Figure 3**. ***Dot1l*-KO in male germ cells leads to multiple spermiogenesis defects including flagellar**
1002 **abnormalities and incomplete sperm chromatin reorganization and compaction**

1003 A) Representative pictures of *Dot1l*-KO and CTL epididymal spermatozoa. The black arrow indicates an
1004 abnormal sperm head (without apical hook) and white arrows indicate thinning of the flagellum. Scale
1005 bars represent 10µm. B) Ultrastructure pictures (electron microscopy) from epididymal spermatozoa
1006 showing multiple abnormalities in *Dot1l*-KO compared to CTL: disorganized microtubules (blue arrow),
1007 impaired nuclear compaction (top panels) and increased cytoplasmic retention (bottom right panel).
1008 Scale bars represent 1µm. C) Scatter plots (mean values following angular transformation +/- standard
1009 deviation) of the percentage of motile and progressively motile spermatozoa in *Dot1l*-KO and CTL adult
1010 mice (N= 12 for CTL and 10 for *Dot1l*-KO) obtained following CASA (computer-assisted sperm analysis).
1011 Three stars indicate a p-value <0.0005 (Mann Whitney test performed after angular transformation of
1012 the percentages). D) Scatter plots showing the percentage of testicular tubules with TUNEL-positive
1013 elongating/condensing spermatids (ES) (mean per animal + standard error of the mean, N=5 for CTL
1014 and 6 for *Dot1l*-KO). Two stars indicate a p-value <0.005 (unpaired t-test performed after angular
1015 transformation of percentages). A representative picture of *Dot1l*-KO testicular sections following
1016 TUNEL assay is shown on the left. TUNEL positive elongating/condensing spermatids are visible inside
1017 the tubule (in green, white arrowhead). DAPI (blue) was used to stain nuclei. Scale bar indicates 20µm.
1018 E) Western blot detection of histones H3 and TH2B in spermatozoa from *Dot1l*-KO and CTL males. The
1019 same quantity of material was loaded in each well (i.e. extracts from 2 million spermatozoa). NS
1020 indicates a non-specific band also observed on the membrane stained with Ponceau (see Appendix
1021 FigS3C). F) Western blot detection of transition protein 2 (TNP2) in spermatozoa from *Dot1l*-KO and
1022 CTL males. The same quantity of material was loaded in each well (i.e. extracts from 2 million
1023 spermatozoa). G) Coomassie-stained protamine extracts from CTL and *Dot1l*-KO spermatozoa
1024 following acid urea gel electrophoresis (same gel, two different intensities). The same quantity of
1025 material has been loaded in each well (i.e. extracts from 1.4 million spermatozoa). Protamine 1 and 2
1026 bands (PRM1 and PRM2, respectively) are detected at the bottom of the gel. The rectangle highlights
1027 the bands that are likely immature forms of Protamine 2 (i.e. non-cleaved precursor forms). The right
1028 panel shows a western blot detection using anti-PRM2 antibody which confirms that one of the high

1029 molecular weight band only observed in *Dot1l*-KO spermatozoa is an immature form of Protamine 2
1030 (Pre-PRM2). The corresponding coomassie-stained gel is also shown. H) Quantification of histones
1031 TH2B and H3 (N= 11 CTL and 10 KO), of TNP2 (N= 8 CTL and 8 KO) and of PRM1/PRM2 ratio (N= 3 CTL
1032 and 3 KO) in *Dot1l*-KO and CTL spermatozoa, related to Fig 3E-G. The data shown are normalized to
1033 control mean values (+ standard error of the mean). One star indicates a p-value <0.05, and three stars,
1034 a p-value <0.0005 (unpaired t-tests). A.U. = arbitrary units. See also Fig EV2 and Appendix FigS3.

1035 **Figure 4. *Dot1l*-KO modifies the chromatin of elongating/condensing spermatids**

1036 Bar plots showing the quantification of post-translational modifications (PTMs) in histones H3 and H4
1037 in ES (elongating/condensing spermatids) by LC-MS/MS. After normalization to be at constant amount
1038 of histone H3 or H4 in each analyzed sample (see Material and methods), mass spectrometry signals
1039 were divided by the average signal in both conditions (CTL and KO), so as to be able to represent all
1040 peptides in the same figure, whatever their MS intensity. Quantitative data obtained on individual
1041 biological replicates were plotted as dots, and the height of the bars indicates the average value over
1042 technical replicates. T-tests were performed to estimate the possible significant difference of modified
1043 peptide abundances between the two genotypes. One star indicates a p-value <0.05, two stars a p-
1044 value<0.005 and three stars a p-value <0.0005. When interpreting our mass spectrometry data against
1045 the database MS_histoneDB, we were able to identify various H3 variants, namely canonical H3 and
1046 variants H3.3, testis-specific H3t and H3mm13. "H3" indicates sequences shared among several
1047 variants; "H3.3", "H3t" or "H3mm13", each variant. A.U. = arbitrary units. See also Figs EV3, 4 and
1048 Appendix FigS4.

1049 **Figure 5. *Dot1l*-KO leads to the deregulation of genes involved in flagellum function, transcription**
1050 **regulation, chromatin organization, mitochondria function and apoptosis.**

1051 A) Multi-dimensional scaling plot on the 500 top genes in *Dot1l*-KO vs. CTLs primary spermatocytes
1052 (SC), secondary spermatocytes (SCII) and round spermatids (RS) using pairwise gene selection. B) MD
1053 plot of the genes found deregulated in *Dot1l*-KO vs. CTLs SC, SCII and RS, using differential gene
1054 expression analyses with two different parameters (FDR<0.05 and p-value<0.05). C) H3K79me2
1055 enrichment profile at deregulated genes (same parameters as in B). D) H3K79me2 enrichment profile
1056 at selected deregulated genes, in two biological replicates of ChIP-Seq performed in wild type RS
1057 (Rep#1 and 2. The input value is shown in grey. E) GSEA analysis of RNA-Seq data from *Dot1l*-KO vs CTL
1058 SC, SCII and RS. The figure shows all the biological pathways found significantly downregulated in
1059 *Dot1l*-KO primary spermatocytes (SC), secondary spermatocytes (SCII) and round spermatids (p<0.05),
1060 ranked by their enrichment score (ES). See also Fig EV5 and Appendix FigS5.

1061 ## Expanded View Figure legends

1062 **Figure EV1. Immunofluorescence detection of H3K79me2 on testicular sections from adult CTL or**
1063 ***Dot1l*-KO mice**. H3K79me2 signal is shown in green. DAPI (grey or blue) was used to stain nuclei. Lectin
1064 (pink) was used to stain acrosome. Scale bar indicates 20µm.

1065 **Figure EV2. A) Scatter plots showing the quantification of sperm abnormalities**. Stars indicate
1066 significant differences obtained using t-tests after angular transformation of the percentages, with the
1067 following p-values. One star indicates a p-value <0.05, two stars a p-value<0.005 and three stars a p-
1068 value <0.0005 (N= 4 to 5 CTL and 4 DOT1L-KO males). **B**) **Motility parameters from *Dot1l*-KO and CTL**
1069 **spermatozoa following CASA** (computer-assisted sperm analyses) (N= 12 CTL and 10 KO males).
1070 Specifically, *Dot1l*-KO spermatozoa are slower and more static. They have a more linear movement
1071 (LIN) and a decreased straightness (STR), decreased lateral displacements of their heads (ALH) with a
1072 lower curvilinear velocity (VCL) resulting in a straight-line velocity (VSL) similar to CTL spermatozoa but
1073 a higher Average Path Velocity (VAP). Stars indicate significant differences obtained using Mann
1074 Whitney t-tests after angular transformation of the percentages (** with a p-value <0.01, *** with a
1075 p-value <0.001, **** with a p-value <0.0001, 'ns' indicates non-significance). The Beat Cross Frequency
1076 (BCF) of CTL and *Dot1l* -KO spermatozoa is similar.

1077 **Figure EV3. Confirmation of a decrease in H4 acetylation in elongating spermatids (ES)** by
1078 **immunofluorescence.** Representative pictures of immunofluorescence detection of acH4 (anti-poly-
1079 H4ac, green) on stage XI testicular sections. At this stage, acH4 level is strong in CTL elongating
1080 spermatids but appears weaker in *Dot1l*-KO. DAPI (blue) was used to stain nuclei and lectin (red) to
1081 stage the acrosome and facilitates tubule staging. Scale bar indicates 20µm.

1082 **Figure EV4. Quantification of histone H3 and H4 PTMs in *Dot1l*-KO and CTL round spermatids (N= CTL**
1083 **and 3 KO).** LC-MS/MS data acquired on H3 and H4 were processed as described in Figure 4. One star
1084 indicates a p-value <0.05, two stars a p-value<0.005 and three stars a p-value <0.0005, obtained with
1085 t-tests.

1086 **Figure EV5. GSEA analysis of RNA-seq data from *Dot1l*-KO vs CTL SC, SCII and RS.** The figure shows all
1087 the "cellular components" found significantly downregulated in *Dot1l*-KO primary spermatocytes (SC),
1088 secondary spermatocytes (SCII) and round spermatids (p<0.05), ranked by their enrichment score (ES).

1089

Fig1

A

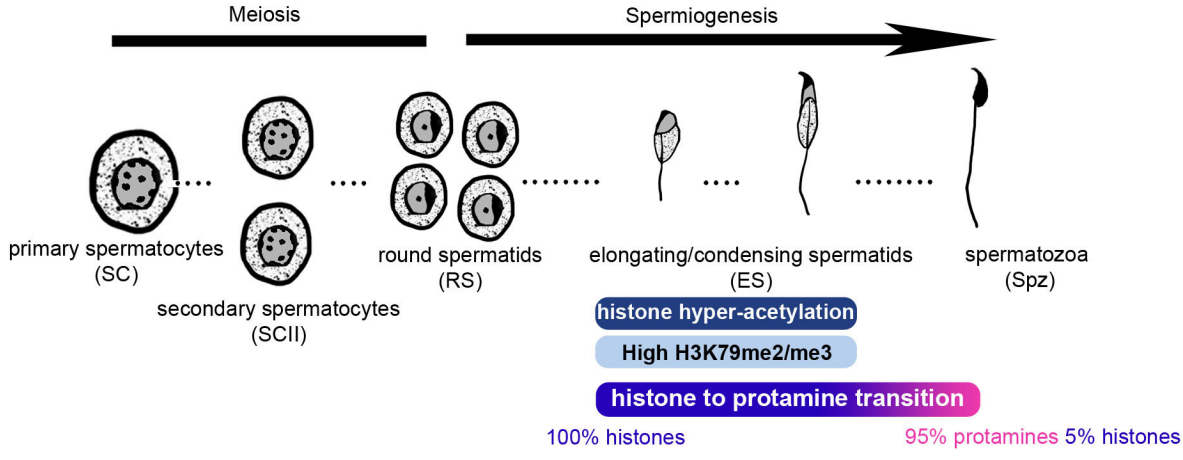
Meiosis
Spermiogenesis
primary spermatocytes
(SC)
secondary spermatocytes
(SCII)
round spermatids
(RS)
elongating/condensing spermatids
(ES)
spermatozoa
(Spz)
histone hyper-acetylation
High H3K79me2/me3
histone to protamine transition
100% histones
95% protamines 5% histones

B

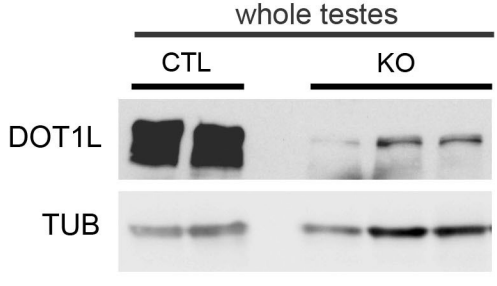
whole testes
CTL
KO
DOT1L
TUB

C

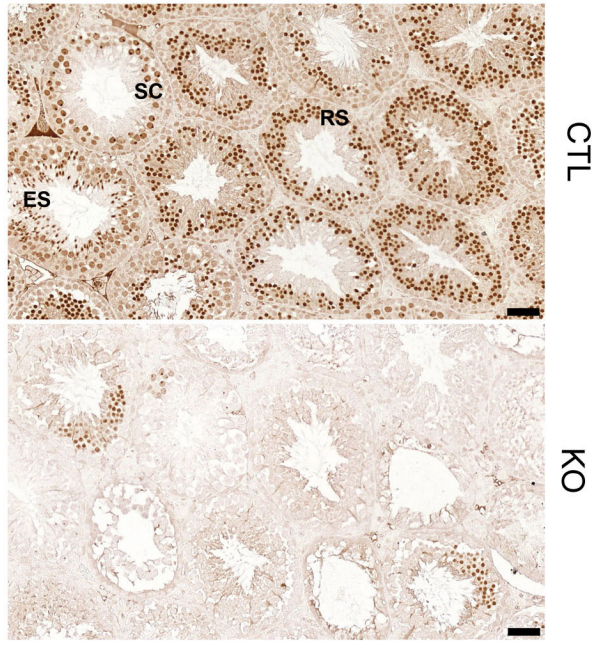
SC
RS
ES
CTL
KO

D

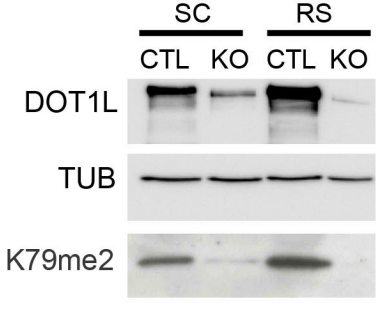
SC
RS
CTL
KO
CTL
KO
DOT1L
TUB
K79me2

Fig. 2

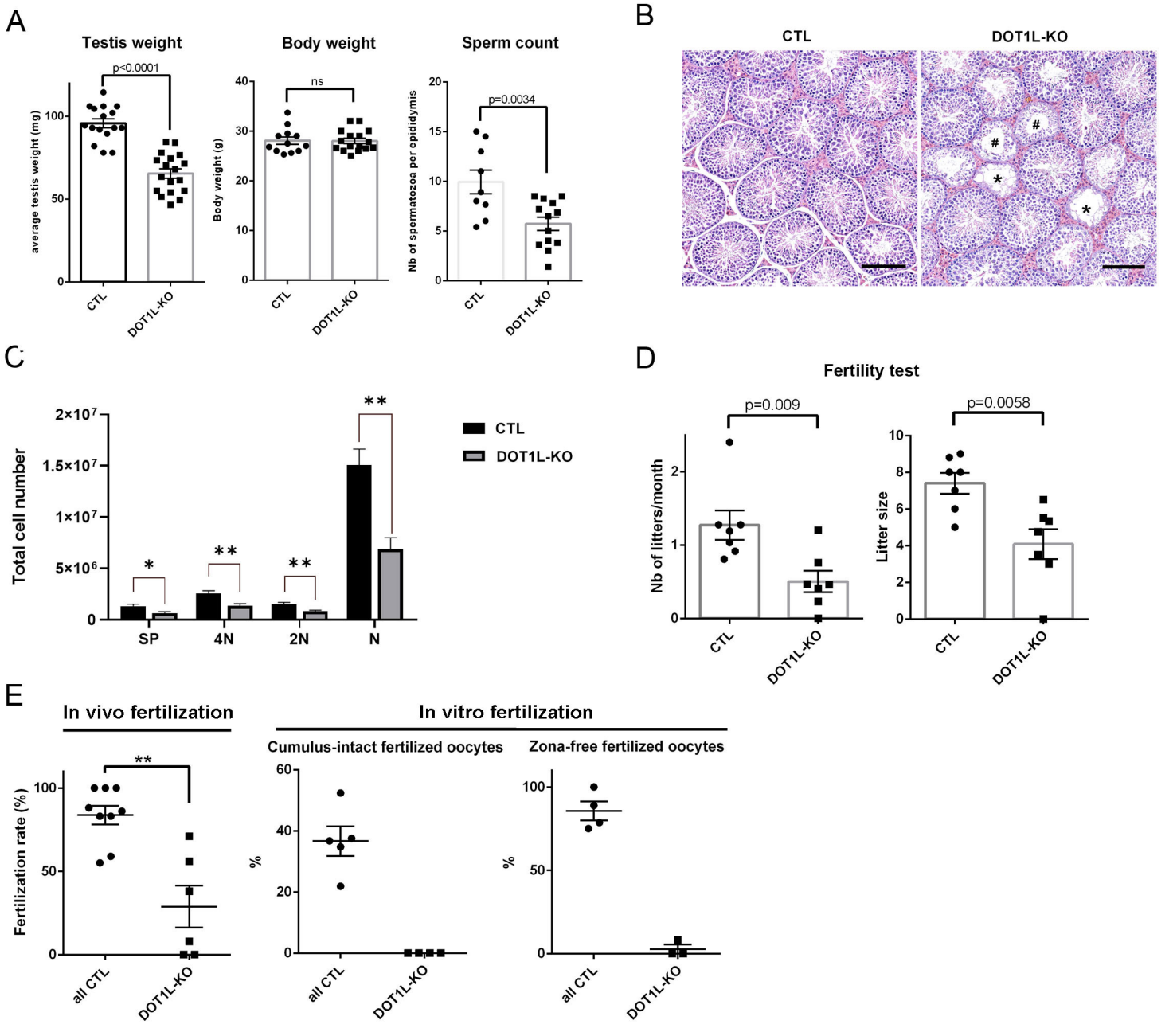
A
Testis weight
p<0.0001
average testis weight (mg)
CTL
DOT1L-KO
Body weight
ns
Body weight (g)
Sperm count
p=0.0034
Nb of spermatozoa per epididymis
B
CTL
DOT1L-KO
C
Total cell number
CTL
DOT1L-KO
SP
4N
2N
N
D
Fertility test
p=0.009
Nb of litters/month
p=0.0058
Litter size
E
In vivo fertilization
Fertilization rate (%)
all CTL
DOT1L-KO
In vitro fertilization
Cumulus-intact fertilized oocytes
Zona-free fertilized oocytes
%

Fig. 3

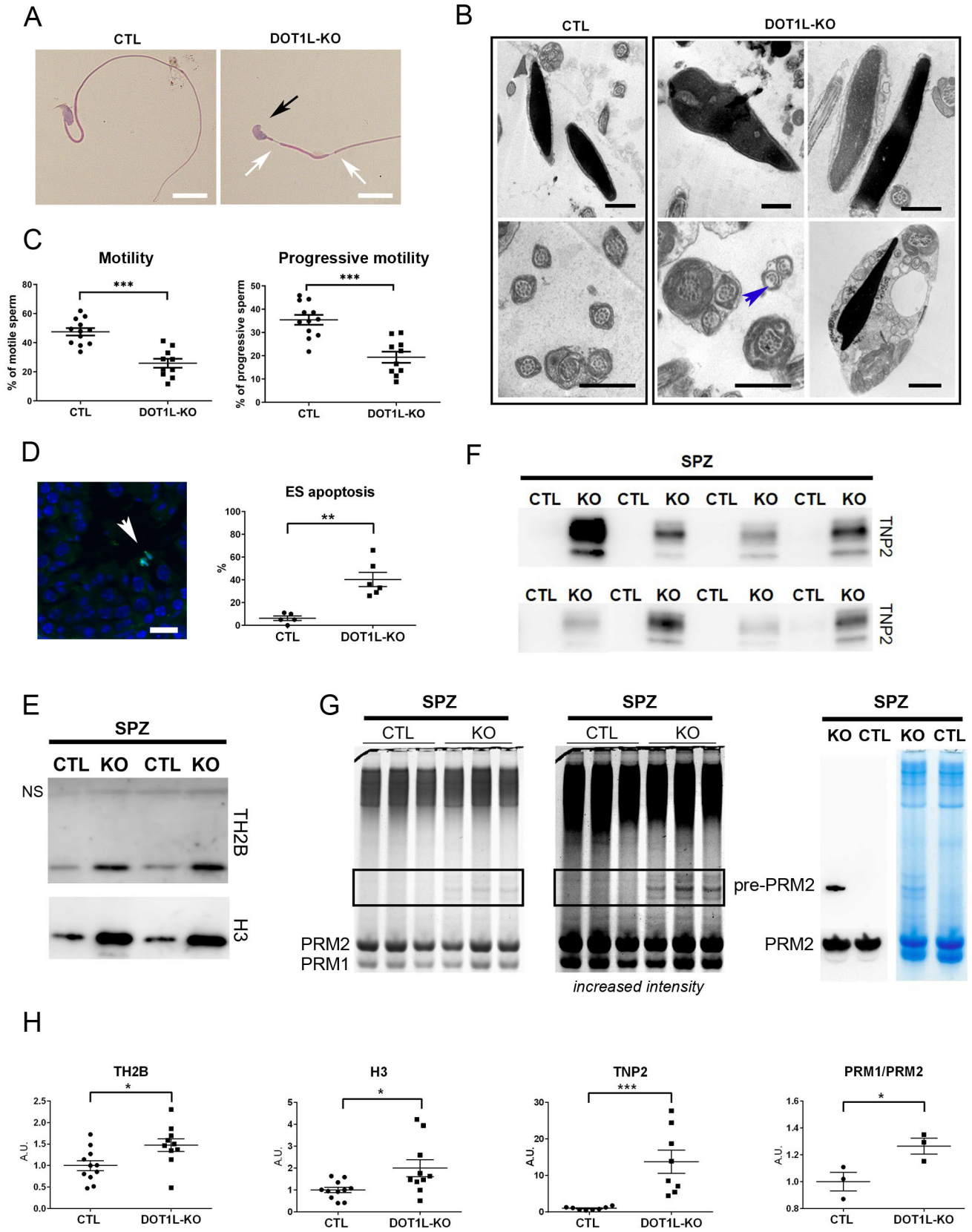
A
CTL
DOT1L-KO
B
CTL
DOT1L-KO
C
Motility
% of motile sperm
***
CTL
DOT1L-KO
Progressive motility
% of progressive sperm
***
CTL
DOT1L-KO
D
ES apoptosis
%
**
CTL
DOT1L-KO
F
SPZ
CTL KO CTL KO CTL KO CTL KO
TNP2
CTL KO CTL KO CTL KO CTL KO
TNP2
E
SPZ
CTL KO CTL KO
NS
TH2B
H3
G
SPZ
CTL KO
PRM2
PRM1
SPZ
CTL KO
increased intensity
SPZ
KO CTL KO CTL
pre-PRM2
PRM2
H
TH2B
A.U.
*
CTL
DOT1L-KO
H3
A.U.
*
CTL
DOT1L-KO
TNP2
A.U.
***
CTL
DOT1L-KO
PRM1/PRM2
A.U.
*
CTL
DOT1L-KO

Fig. 4

A

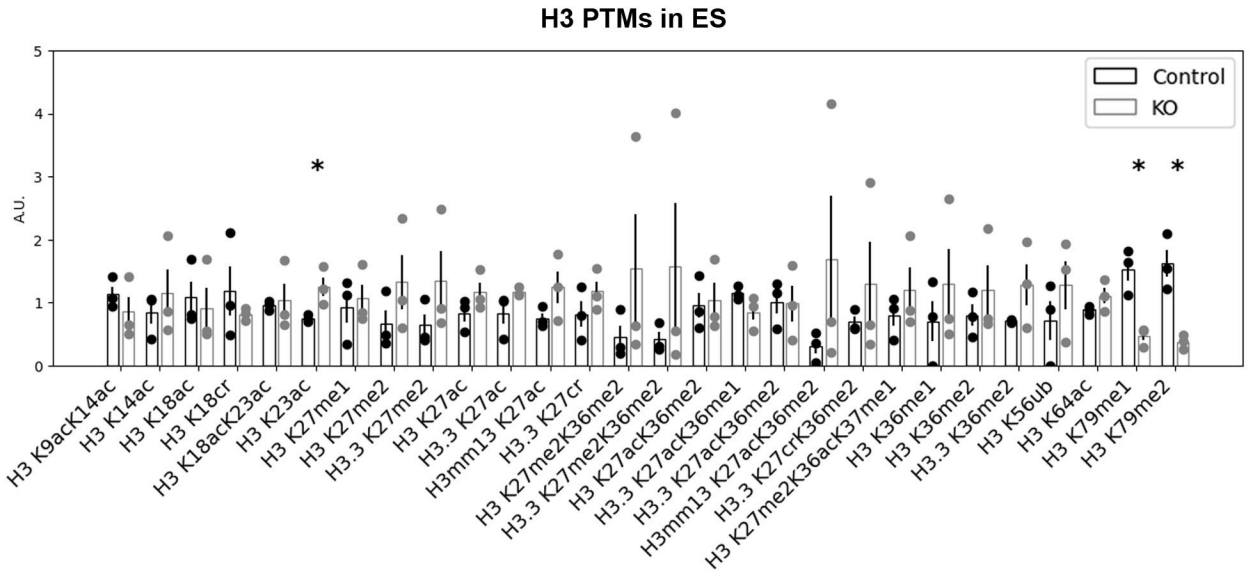
H3 PTMs in ES
Control
KO
A.U.
0
1
2
3
4
5
*
* *
H3 K9acK14ac
H3 K14ac
H3 K18ac
H3 K18cr
H3 K18acK23ac
H3 K23ac
H3 K27me1
H3 K27me2
H3.3 K27me2
H3 K27ac
H3.3 K27ac
H3mm13 K27ac
H3.3 K27cr
H3 K27me2K36me2
H3.3 K27me2K36me2
H3 K27acK36me2
H3.3 K27acK36me1
H3.3 K27acK36me2
H3mm13 K27acK36me2
H3.3 K27crK36me2
H3 K27me2K36acK37me1
H3 K36me1
H3 K36me2
H3.3 K36me2
H3 K56ub
H3 K64ac
H3 K79me1
H3 K79me2

B

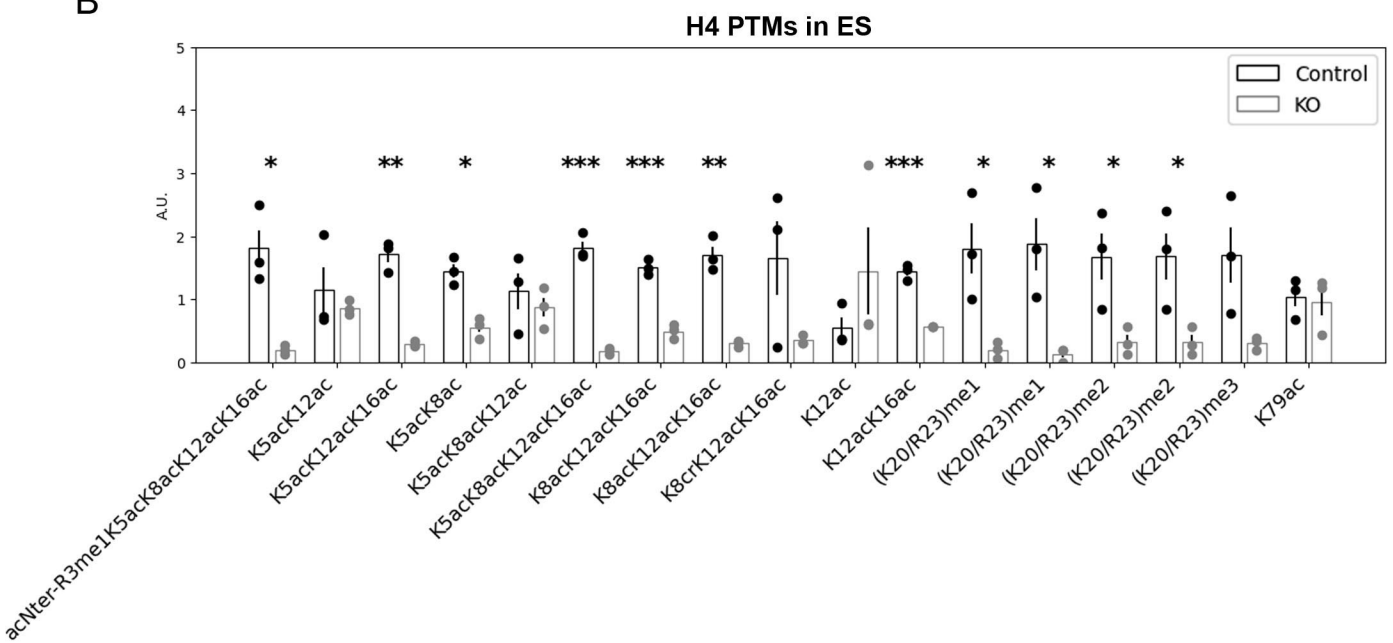
H4 PTMs in ES
Control
KO
A.U.
0
1
2
3
4
5
*
**
*
***
***
**
***
*
*
*
*
acNter-R3me1K5acK8acK12acK16ac
K5acK12ac
K5acK12acK16ac
K5acK8ac
K5acK8acK12ac
K5acK8acK12acK16ac
K8acK12acK16ac
K8acK12acK16ac
K8crK12acK16ac
K12ac
K12acK16ac
(K20/R23)me1
(K20/R23)me1
(K20/R23)me2
(K20/R23)me2
(K20/R23)me3
K79ac

Fig. 5

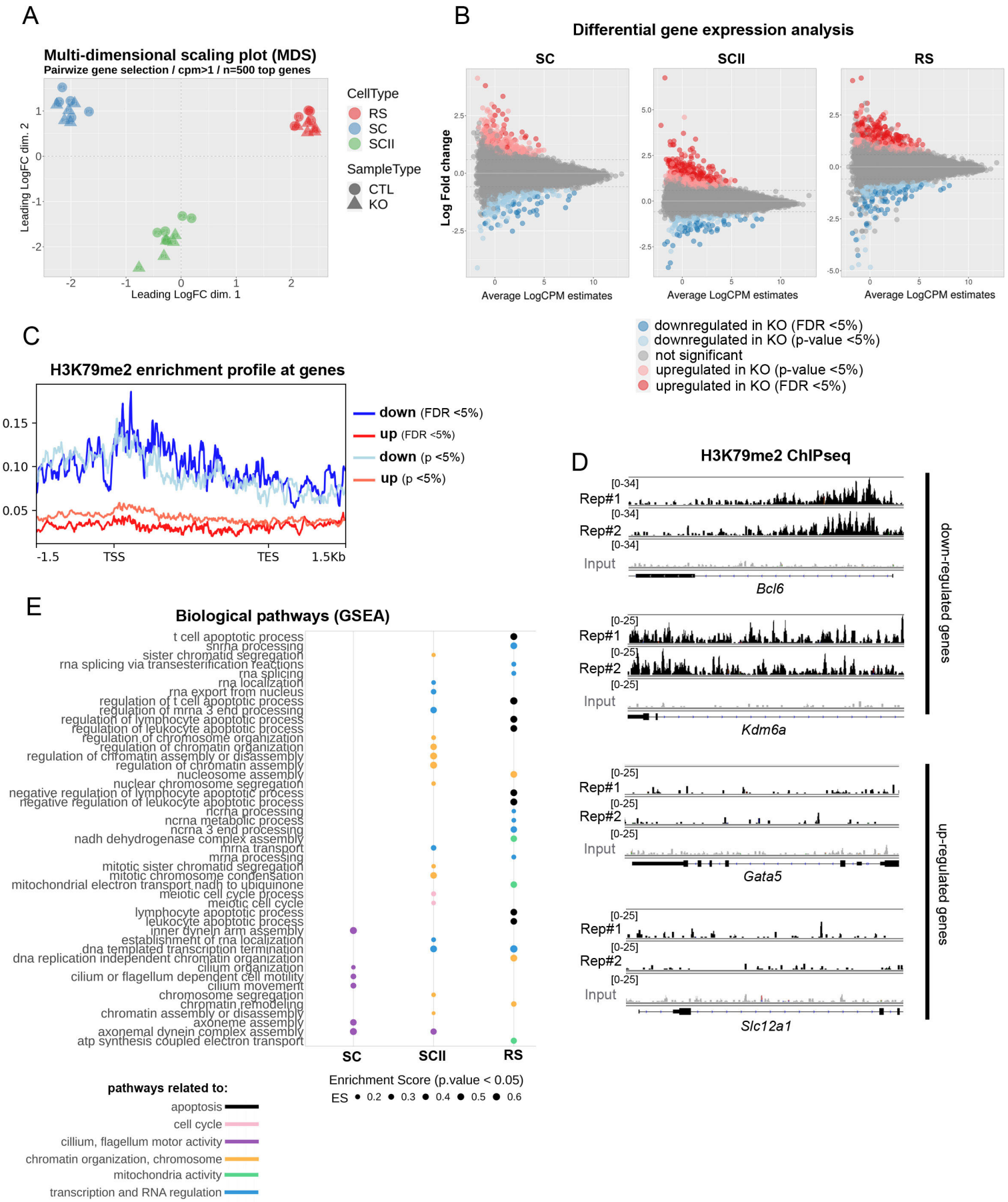
A
Multi-dimensional scaling plot (MDS)
Pairwise gene selection / cpm>1 / n=500 top genes
Leading LogFC dim. 2
Leading LogFC dim. 1
CellType
RS
SC
SCII
SampleType
CTL
KO
B
Differential gene expression analysis
SC
SCII
RS
Log Fold change
Average LogCPM estimates
downregulated in KO (FDR <5%)
downregulated in KO (p-value <5%)
not significant
upregulated in KO (p-value <5%)
upregulated in KO (FDR <5%)
C
H3K79me2 enrichment profile at genes
down (FDR <5%)
up (FDR <5%)
down (p <5%)
up (p <5%)
-1.5
TSS
TES
1.5Kb
D
H3K79me2 ChIPseq
Rep#1
Rep#2
Input
Bcl6
Kdm6a
Gata5
Slc12a1
down-regulated genes
up-regulated genes
E
Biological pathways (GSEA)
t cell apoptotic process
snrna processing
sister chromatid segregation
rna splicing via transesterification reactions
rna splicing
rna localization
rna export from nucleus
regulation of t cell apoptotic process
regulation of mrna 3 end processing
regulation of lymphocyte apoptotic process
regulation of leukocyte apoptotic process
regulation of chromosome organization
regulation of chromatin organization
regulation of chromatin assembly or disassembly
regulation of chromatin assembly
nucleosome assembly
nuclear chromosome segregation
negative regulation of lymphocyte apoptotic process
negative regulation of leukocyte apoptotic process
ncrna processing
ncrna metabolic process
ncrna 3 end processing
nadh dehydrogenase complex assembly
mrna transport
mrna processing
mitotic sister chromatid segregation
mitotic chromosome condensation
mitochondrial electron transport nadh to ubiquinone
meiotic cell cycle process
meiotic cell cycle
lymphocyte apoptotic process
leukocyte apoptotic process
inner dynein arm assembly
establishment of rna localization
dna templated transcription termination
dna replication independent chromatin organization
cilium organization
cilium or flagellum dependent cell motility
cilium movement
chromosome segregation
chromatin remodeling
chromatin assembly or disassembly
axoneme assembly
axonemal dynein complex assembly
atp synthesis coupled electron transport
SC
SCII
RS
Enrichment Score (p.value < 0.05)
ES 0.2 0.3 0.4 0.5 0.6
pathways related to:
apoptosis
cell cycle
cillium, flagellum motor activity
chromatin organization, chromosome
mitochondria activity
transcription and RNA regulation

Figure EV1

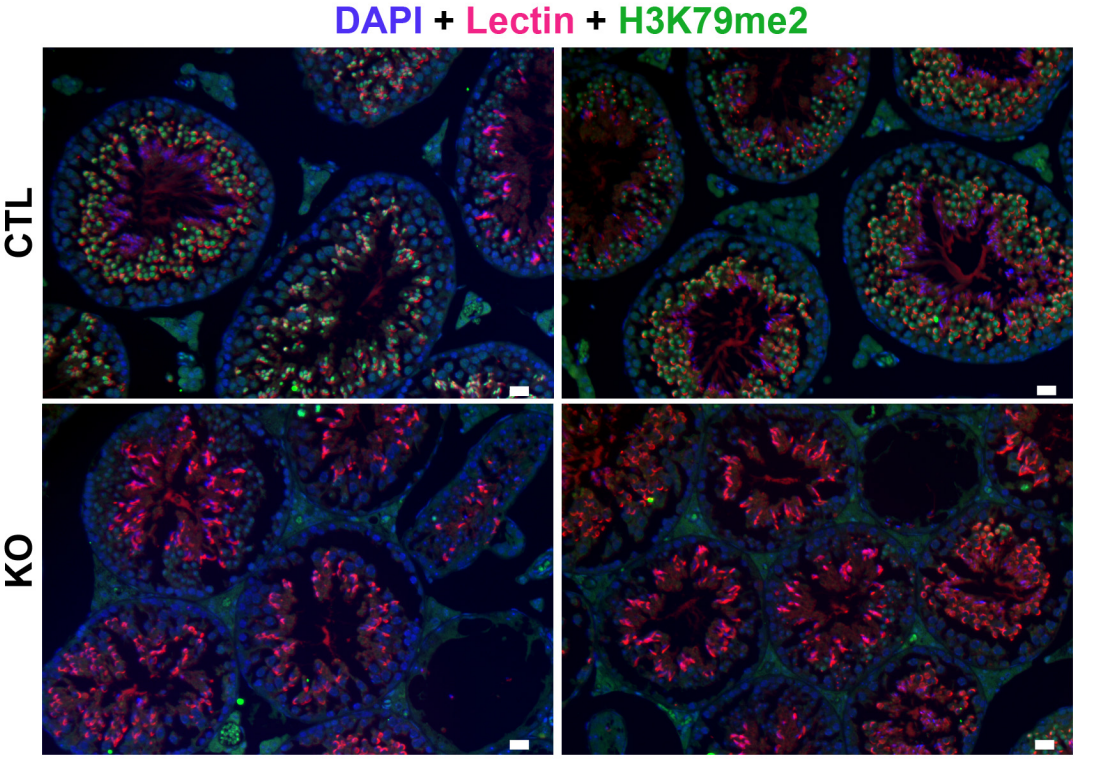

Figure EV2

A

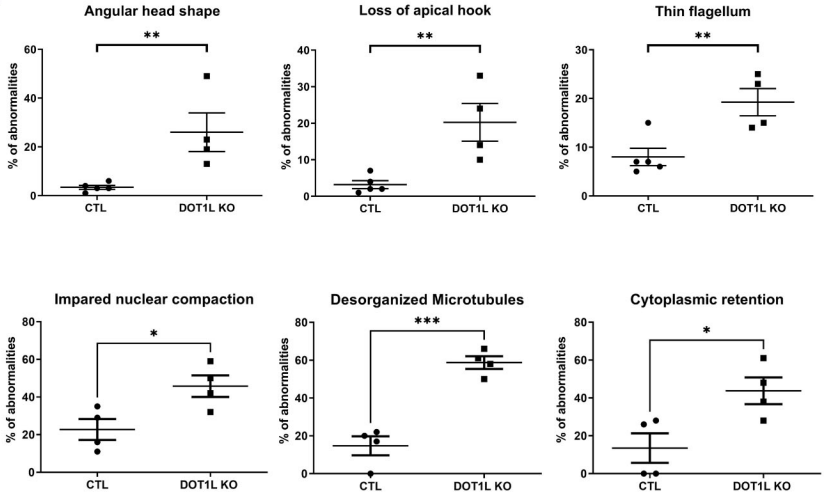

B

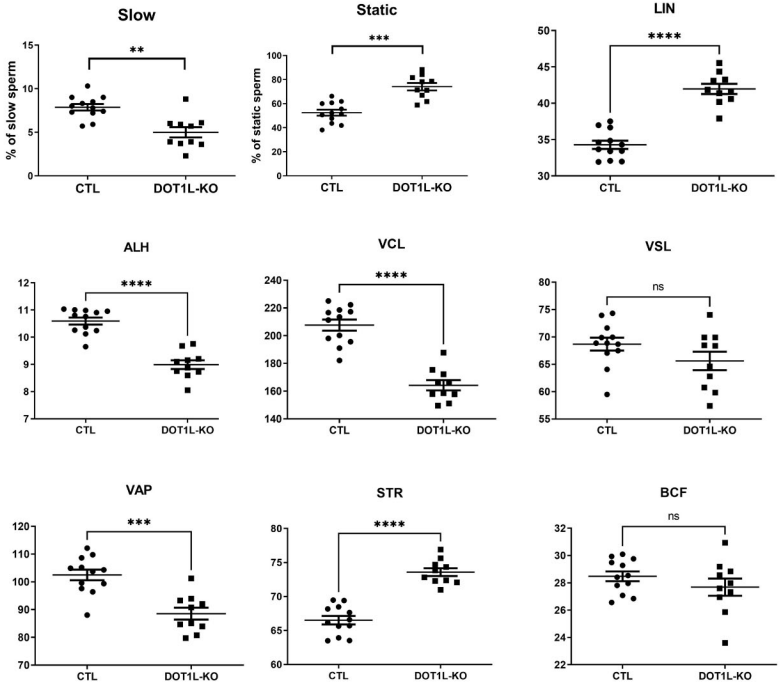

Figure EV3

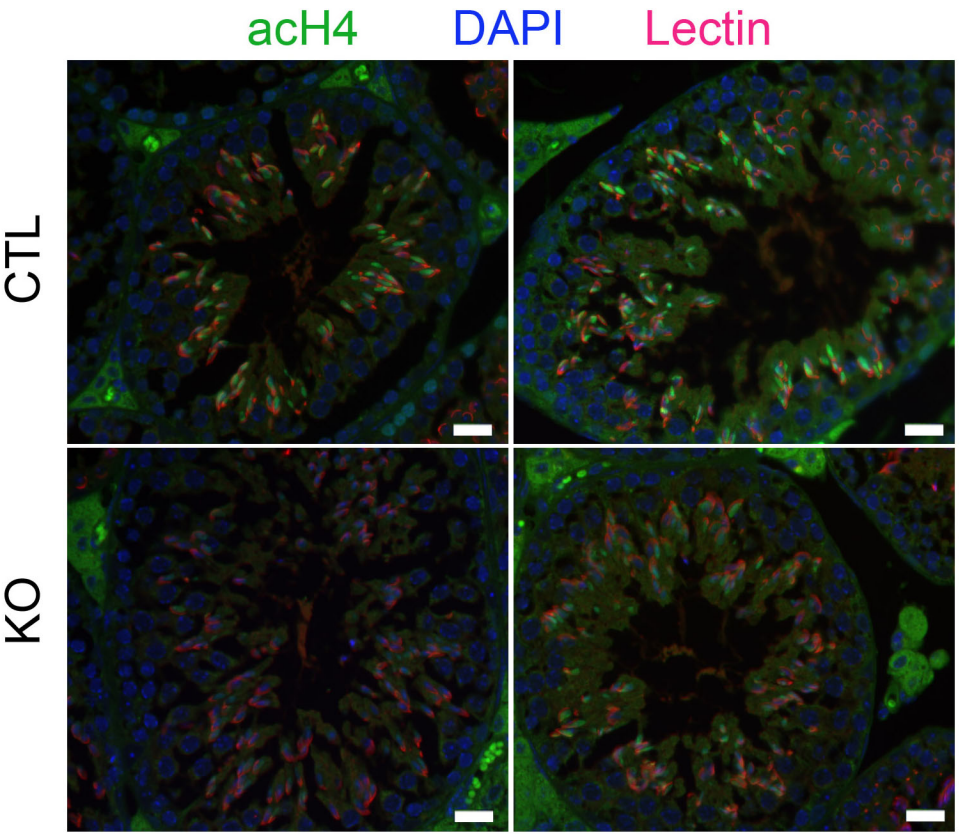

Figure EV4

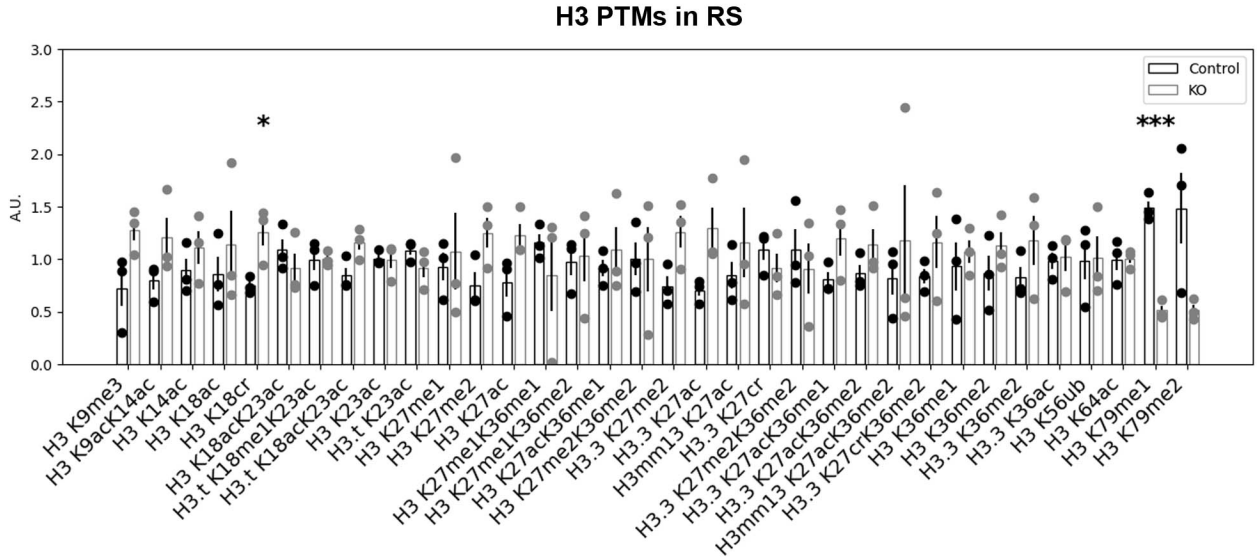
H3 PTMs in RS
Control
KO
A.U.
*
***
H3 K9me3
H3 K9acK14ac
H3 K14ac
H3 K18ac
H3 K18cr
H3 K18acK23ac
H3.t K18me1K23ac
H3.t K18acK23ac
H3 K23ac
H3.t K23ac
H3 K27me1
H3 K27me2
H3 K27ac
H3 K27me1K36me1
H3 K27me1K36me2
H3 K27acK36me1
H3 K27me2K36me2
H3.3 K27me2
H3.3 K27ac
H3mm13 K27ac
H3.3 K27cr
H3.3 K27me2K36me2
H3.3 K27acK36me1
H3.3 K27acK36me2
H3mm13 K27acK36me2
H3.3 K27crK36me2
H3 K36me1
H3 K36me2
H3.3 K36me2
H3.3 K36ac
H3 K56ub
H3 K64ac
H3 K79me1
H3 K79me2

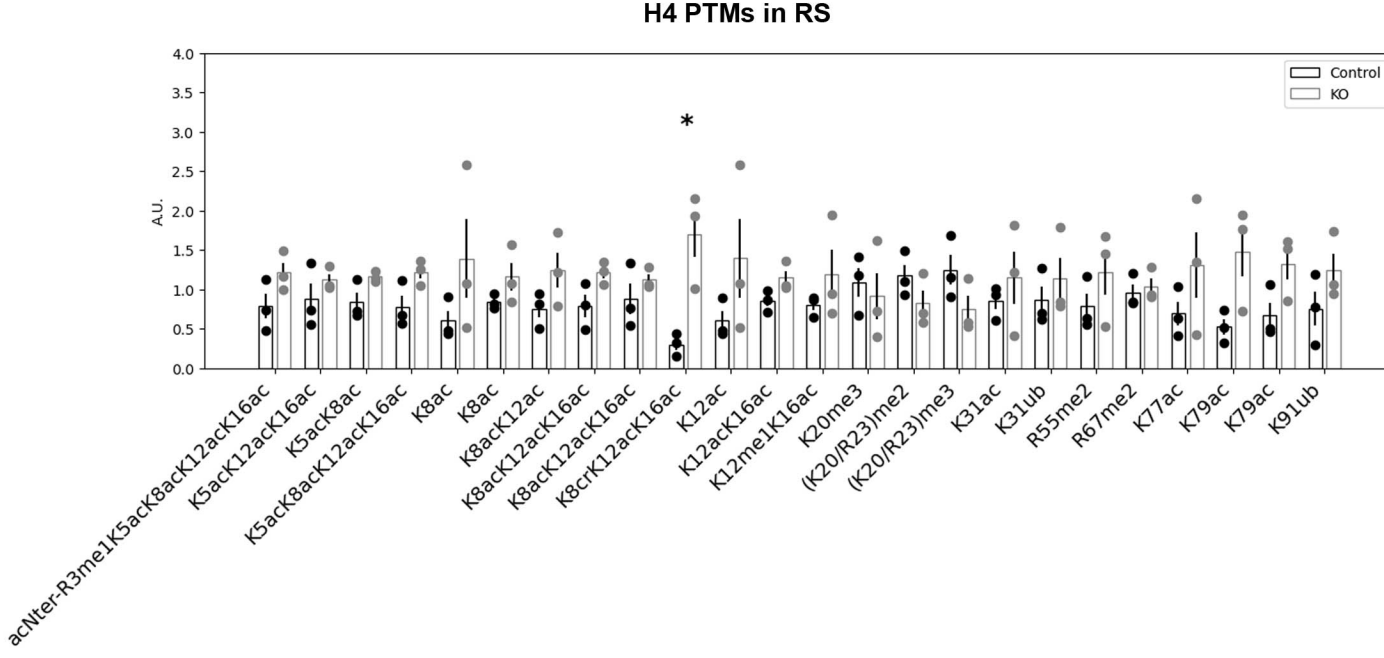
H4 PTMs in RS
Control
KO
A.U.
*
acNter-R3me1K5acK8acK12acK16ac
K5acK12acK16ac
K5acK8ac
K5acK8acK12acK16ac
K8ac
K8ac
K8acK12ac
K8acK12acK16ac
K8acK12acK16ac
K8crK12acK16ac
K12ac
K12acK16ac
K12me1K16ac
K20me3
(K20/R23)me2
(K20/R23)me3
K31ac
K31ub
R55me2
R67me2
K77ac
K79ac
K79ac
K91ub

Figure EV5

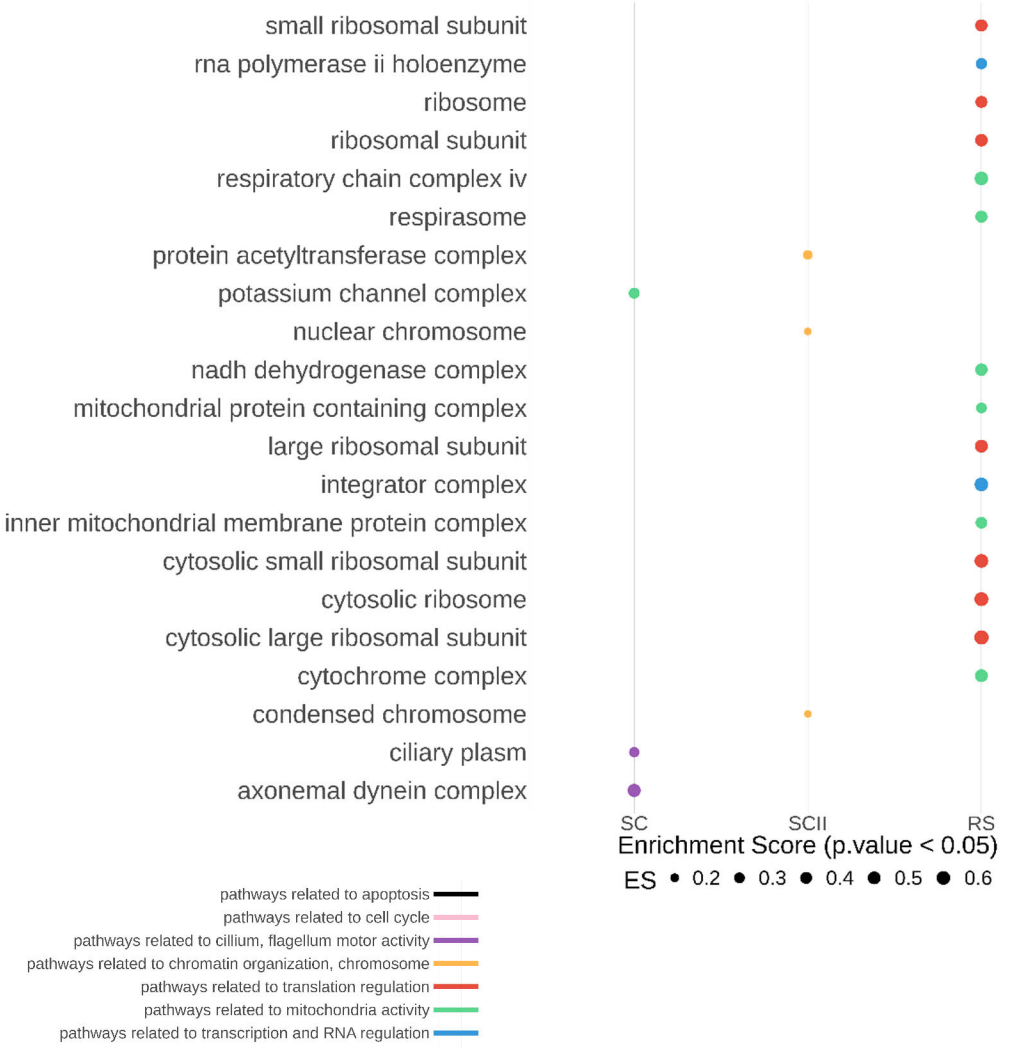
small ribosomal subunit
rna polymerase ii holoenzyme
ribosome
ribosomal subunit
respiratory chain complex iv
respirasome
protein acetyltransferase complex
potassium channel complex
nuclear chromosome
nadh dehydrogenase complex
mitochondrial protein containing complex
large ribosomal subunit
integrator complex
inner mitochondrial membrane protein complex
cytosolic small ribosomal subunit
cytosolic ribosome
cytosolic large ribosomal subunit
cytochrome complex
condensed chromosome
ciliary plasm
axonemal dynein complex
SC
SCII
RS
Enrichment Score (p.value < 0.05)
ES
0.2
0.3
0.4
0.5
0.6
pathways related to apoptosis
pathways related to cell cycle
pathways related to cillium, flagellum motor activity
pathways related to chromatin organization, chromosome
pathways related to translation regulation
pathways related to mitochondria activity
pathways related to transcription and RNA regulation